construction materials

MDPI

Article

Mechanical, Durability, and Environmental Performance of Limestone Powder-Modified Ultra-High-Performance Concrete

Yashovardhan Sharma, Meghana Yeluri and Srinivas Allena *

Department of Civil and Environmental Engineering, Cleveland State University, Cleveland, OH 44115, USA; y.sharma@vikes.csuohio.edu (Y.S.); y.meghana@vikes.csuohio.edu (M.Y.)
* Correspondence: s.allena@csuohio.edu

Abstract

Ultra-high-performance concrete (UHPC) delivers outstanding durability and strength but typically relies on high Portland cement content. This study evaluates a 20% cement replacement with limestone powder (LP) in UHPC and benchmarks performance under two curing regimes: moist curing (MC) and warm bath curing at 90 °C (WB). Metrics include workability, compressive and flexural behavior, shrinkage, freeze–thaw resistance, chloride transport (surface resistivity, RCPT), material cost, and embodied CO_2. LP improved fresh behavior: flow increased by 14.3% in plain UHPC and 33% in fiber-reinforced UHPC (FR-UHPC). Compressive strengths remained in the UHPC range at 28–56 days (approximately 142–152 MPa with LP), with modest penalties versus 0%-LP controls (about 2–5% depending on age and curing). Under WB at 56 days, controls reached 154 MPa (plain) and 161 MPa (FR-UHPC), while LP mixes achieved 145.2 MPa (plain) and 152.0 MPa (FR-UHPC). Flexural performance was reduced with LP: for FR-UHPC, 28-day MOR under MC was reduced from 15.5 MPa to 12.7 MPa and under WB from 14.3 MPa to 10.3 MPa; toughness under MC was reduced from 74.4 J to 51.1 J. Durability indicators were maintained or improved despite these moderate strength reductions. After 300 rapid freeze–thaw cycles, all mixtures retained relative dynamic modulus near 100–103%, with negligible MOR losses in LP mixes (plain UHPC: −1.1% with LP versus −4.7% without; FR-UHPC: −3.7% versus −8.1%). Chloride transport resistance improved: at 56 days under MC, surface resistivity increased from 558 to 707 kΩ·cm in plain UHPC and from 252 to 444 kΩ·cm in FR-UHPC; RCPT for LP mixes was 139 C (MC) and 408 C (WB), about 14–23% lower than respective controls. Drying shrinkage was reduced by roughly 23% (plain) and 28% (FR-UHPC). Sustainability and cost outcomes were favorable: embodied CO_2 was reduced by 18.8% (plain) and 15.5% (FR-UHPC), and material cost was reduced by about 4.5% and 2.0%, respectively. The main shortcomings are moderate reductions in compressive and flexural strength and toughness, particularly under WB curing, which should guide application-specific limits and design factors.

Keywords: UHPC; limestone powder; mechanical properties; durability; shrinkage; sustainability

check for updates

Received: 29 September 2025
Revised: 20 November 2025
Accepted: 5 December 2025
Published: 10 December 2025

Citation: Sharma, Y.; Yeluri, M.; Allena, S. Mechanical, Durability, and Environmental Performance of Limestone Powder-Modified Ultra-High-Performance Concrete. *Constr. Mater.* **2025**, *5*, 90. https://doi.org/10.3390/constrmater5040090

Copyright: © 2025 by the authors. Licensee MDPI, Basel, Switzerland. This article is an open access article distributed under the terms and conditions of the Creative Commons Attribution (CC BY) license (https://creativecommons.org/licenses/by/4.0/).

1. Introduction

Ultra-high-performance concrete (UHPC), also termed reactive powder concrete (RPC) [1], was first developed by the Bouygues laboratory in France [2]. Distinguished by its very low water-to-cementitious materials ratio (w/cm) and absence of coarse aggregate [3], UHPC delivers exceptional mechanical strength, durability, and service life, making it

suitable for infrastructure applications. However, UHPC typically contains three times more cement than conventional concrete [4–6], significantly contributing to the cement sector's 8–9% share of global anthropogenic CO_2 emissions [7]. Under UHPC's low w/cm ratio, only 52–61% of cement hydrates [8], leaving a considerable fraction unreacted [9,10] and reducing its overall material efficiency.

Studies have reported the positive effects of SCMs, such as silica fume (SF) and fly ash (FA) on the compressive strength, workability, and shrinkage properties of UHPC [11–16]. Partial replacement of cement with SCMs has proven effective in reducing the carbon footprint of concrete production [17]. SCMs can satisfy UHPC's performance requirements, including achieving high compressive strength, while simultaneously lowering embodied CO_2 emissions associated with binder production [18,19]. Research has also shown that supplementary mineral fillers such as limestone powder (LP) can provide additional benefits in UHPC [20,21]. LP is attractive due to its low inherent CO_2 emissions, abundant availability, and low cost [22]. Studies have reported a significant increase in UHPC paste flowability with partial replacement of Portland cement (PC) by LP, corroborating earlier findings [23–25]. LP is often considered as a mineral plasticizer that can improve the workability of UHPC mixtures [17].

LP can fill micro-voids and improve particle packing, thereby enhancing system packing density [26] and contributing to early-age compressive strength gains [26]. However, several studies have reported that LP may reduce compressive strength of UHPC at certain replacement levels. For example, Yang et al. [27] observed a 4.2% reduction in 7-day compressive strength when 14% LP (with 24% FA and 12% SF) replaced cement, relative to a reference mixture with only SF and FA. The reduction has been attributed to simultaneous acceleration of hydration and dilution of the cement matrix, which lowers the overall heat of hydration [27].

Physical and durability studies on UHPC with LP have reported mixed outcomes [27,28]. LP can reduce shrinkage in UHPC by lowering total cement content [17,18], yet its influence on porosity appears dosage dependent. Li et al. [17], reported porosity reductions (versus control) at LP contents up to 60%, likely due to filler-induced densification. In contrast, Ding et al. [28] observed increased porosity at higher LP contents, underscoring the potential for dilution effects when inactive fillers replace reactive binder.

Despite these insights, the full spectrum of mechanical and durability responses of UHPC incorporating LP remains insufficiently characterized. This study evaluates the effect of replacing 20% of cement with LP on UHPC properties, including shrinkage; compressive, tensile, and flexural strengths; modulus of elasticity; Poisson's ratio; and toughness. Durability metrics assessed include freeze–thaw resistance, chloride penetrability (rapid chloride permeability), and surface resistivity. In addition, the study quantifies material cost and embodied CO_2 to provide a holistic assessment of performance and sustainability.

2. Materials and Methods

2.1. Materials

Type IL Portland cement (PLC) along with silica fume (SF) and fly ash (FA) as SCMs, and limestone powder (LP) as mineral filler were used in this study. Their chemical compositions and physical properties are presented in Table 1. Figure 1 illustrates the particle size distribution of cement, SF, FA, and LP.

As shown in Figure 1, the particle size of cement ranged from 0.05 to 71 μm, while limestone powder (LP) exhibited a finer and narrower distribution between 0.01 and 36 μm. The relatively small and uniform particle size of LP allows it to effectively fill voids between cement grains, improving packing density and matrix homogeneity through the filler effect. This physical refinement enhances interparticle contact and supports secondary

hydration by providing nucleation sites for hydration products. Silica fume (SF), with ultrafine particles mostly below 1 µm, further densifies the microstructure by filling nano-scale pores and contributing pozzolanic reactivity, while fly ash (FA), with sizes between 1 and 30 µm and a spherical morphology, enhances workability through a ball bearing effect and offers long-term strength gain [29,30]. The combined gradation of cement, LP, SF, and FA yields a dense, well-packed particle system that may improve flowability, mechanical strength, and durability of UHPC, consistent with the observations of Li et al. [17] and Ullah et al. [29,31].

Table 1. Chemical composition and physical properties of cementitious materials used.

Chemical Compounds (%)	Cement	Silica Fume	Fly Ash	LP
SiO_2	20.2	18.9	38.03	1
Al_2O_3	4.3	4.4	18.44	0.15
Fe_2O_3	2.8	2.5	5.16	0.15
CaO	63.8	63.1	16.05	-
MgO	1.6	1.6	3.73	-
SO_3	0.35	3	3.3	-
Na_2O	-	0.34	9.2	-
K_2O	-	-	0.96	-
$MgCO_3$	-	-	-	44.3
$CaCO_3$	-	91	-	54.2
$CaSO_4$ $2H_2O$		-		
Mn		-		
S	-	-	-	-
Loss on ignition	0.88	5.4	2.1	-
Insoluble residue	0.34	-	-	-
Relative density	3.15	3.15	2.58	1.28
moisture content (%)	-	-	0.2	0.2
Blaine fineness (m^2/kg)	401	-	-	-

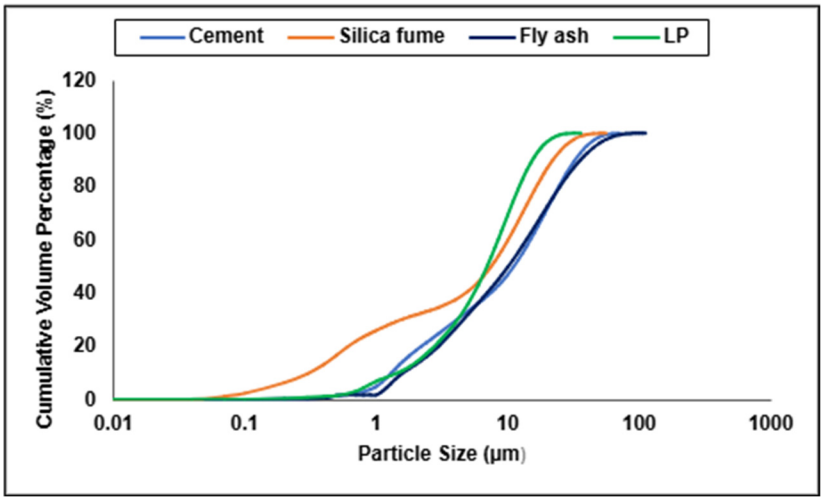


Figure 1. Particle size distribution of cement, SF, FA, and LP.

Locally sourced natural river sand, conforming to ASTM #4 with a maximum particle size of 4.75 mm, served as the fine aggregate. To enhance ductility, straight steel fibers with a length of 13 mm and an aspect ratio of 65 were incorporated. A polycarboxylate-based high-range water-reducing admixture (HRWRA) was used to ensure the desired workability of the UHPC mixtures.

2.2. Mixture Proportioning, Specimen Preparation and Testing

The reference plain (no steel fibers) and fiber-reinforced UHPC mixtures without LP were developed in our previous study [32] and were subsequently modified by replacing 20% cement (by mass) with LP to produce LP-modified UHPC mixtures. The w/cm ratio was kept constant at 0.15 and the HRWRA dosage used was 45 L/m^3. SF and FA were used as SCMs in all four mixtures, with their proportions remaining unchanged in all the UHPC mixtures to maintain consistency in the comparative analysis. Several trial mixtures were investigated with varying LP dosages up to 20% replacement of cement. The mixture proportions of these four mixtures are presented in Table 2. UHPC materials were mixed using a vertical shaft mixer operating at 38 rpm. The mixing process, presented in Figure 2, began with the dry blending of sand and cementitious materials for two minutes. Next, 75% of the total mixing water was added, followed by continued mixing until uniform. The HRWRA was then introduced and mixed for an additional five minutes. The remaining 25% of water was subsequently added and mixed for another 5–6 min. For fiber-reinforced mixtures, steel fibers were added at the end, and the mixing continued for 4–5 more minutes until a homogeneous and workable consistency was achieved. The total mixing duration ranged from 15 to 20 min.

Table 2. Curing regimens used for compressive strength and modulus of rupture tests.

Type	Designation	Specification
Moist curing	MC	The specimens were left in the mold for a period of 24 h. Following demolding, they were subsequently relocated to a curing room with controlled temperature and humidity conditions until testing.
Warm bath curing	WB	The specimens were left in the molds for a period of 24 h. Following the demolding, the specimens were then subjected to curing in a water bath maintained at 90 °C until testing.

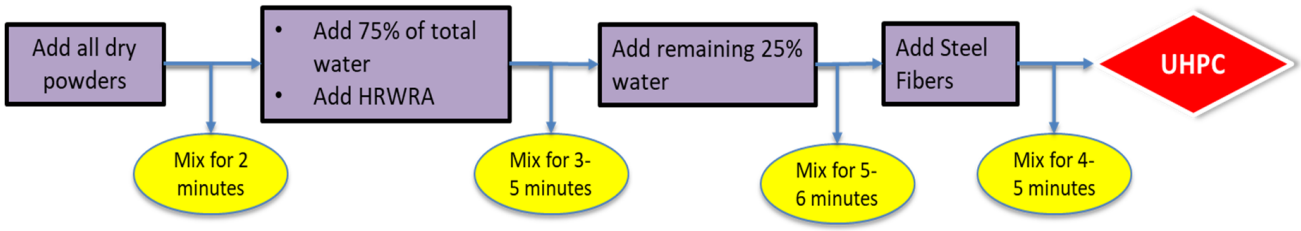


Figure 2. Mixing procedure for UHPC.

After mixing, the fresh concrete was cast into molds and demolded after 24 h. The specimens were then subjected to one of two curing regimens as summarized in Table 3.

Table 3. Proportions of reference and LP-modified plain and fiber-reinforced UHPC mixtures.

Mixture Designation	Cement (kg/m^3)	SF (kg/m^3)	FA (kg/m^3)	LP (kg/m^3)	Sand (kg/m^3)	Steel Fibers (kg/m^3)
UHPC mixtures without LP	890	68	101	0	1110	0
	890	68	101	0	1070	119
UHPC mixtures with 20% LP	712	68	101	178	893	0
	712	68	101	178	853	119

For each experimental test, multiple specimens were prepared and evaluated in accordance with the corresponding ASTM or EN standards. Unless otherwise stated, three to eight specimens, depending on the experiment performed, were tested for each batch and three batches were tested under each curing condition, and the reported values represent the average of all testing results. The variability of the data is presented as error bars in the figures.

To assess statistical significance between mixtures, a Bonferroni post-hoc test was conducted using a 95% confidence level. This approach allows for multiple pairwise comparisons between the UHPC mixtures with and without LP. Differences were considered statistically significant when $p < 0.05$. This criterion indicates that the probability of the observed difference occurring by random chance is less than 5%, confirming significant variation among the tested UHPC mixtures.

2.3. Methods

2.3.1. Workability

The fresh UHPC was placed into the mold in two layers, with each layer tamped 20 times. After leveling the top surface, the mold was carefully lifted and dropped onto the table 25 times within 15 s. The diameter of the spread sample was then measured in two perpendicular directions, and the average flow was recorded in accordance with ASTM C1437 [33].

2.3.2. Compressive Strength

In this study, the compressive strength of UHPC was evaluated using 50 mm cubes in accordance with ASTM C109 [34], after 7 and 28 days of curing under each curing condition.

2.3.3. Split Tensile Strength

Cylinders of size 100 mm by 200 mm were assessed for the split tensile strength of UHPC mixtures in accordance with ASTM C496 [35], with tests conducted at 7 and 28 days for both MC and WB curing regimen. Average split tensile strength was reported based on the split tensile strength of two cylinders.

2.3.4. Modulus of Elasticity and Poisson's Ratio

Modulus of elasticity (MOE) refers to the amount of stress needed to cause unit deformation of a material within its elastic limit, while Poisson's ratio is the ratio of lateral deformation to vertical deformation. Both these parameters are crucial in structural design. In the case of UHPC, testing procedure as per ASTM C469 [36] was used to determine these parameters. A cylinder measuring 100 mm in diameter by 200 mm in height was used and cured for 28 days under both MC and WB curing regimens for each mixture. A compress

meter with an extensometer was attached to the cylinder, and the entire setup was mounted onto a compression machine. The cylinder underwent compression loading until it reached 40% of its ultimate load. The same cylinder was tested three times according to the ASTM C469 [36] standard. The first test served as a system check, while the data from the last two tests were used to calculate the modulus of elasticity and Poisson's ratio.

2.3.5. Flexural Strength

Four prismatic specimens, each measuring 75 × 100 × 400 mm, were cast for each UHPC mixture and cured under MC and WB curing regimens for 28 days to evaluate the flexural behavior of UHPC mixtures. Flexural strength testing was performed according to ASTM C1609 [37]. Two Linear Variable Differential Transformers (LVDT) (Humbolt MFG CO, Elgin, IL, USA) were also mounted at the mid-length of the beam to measure vertical deflection under bending. The loading continued until the net deflection was greater than span/150. Based on the load and displacement data, a stress–strain curve was plotted, and the first crack location was identified. From the test data, modulus of rupture (MOR), which is the first peak strength, peak stress, residual stress at L/600 and L/150 net deflections, where L is the effective length of the beam 305 mm, and toughness of UHPC mixtures were evaluated.

2.3.6. Direct Tension

The direct tensile behavior of UHPC mixtures was evaluated using dog-bone-shaped specimens with a gauge section measuring 38.1 mm in width and 19.1 mm in thickness. An extensometer (Epsilon Technology Corp., Jackson, WY, USA) was attached across the central gauge length to record strain, and loading was applied using a universal testing machine (Tinus Olsen, Horsham, PA, USA) under displacement control until failure. The test was conducted under crosshead displacement control at a rate of 0.00254 mm/s [38]. The specimen was initially subjected to compressive loading up to a stress of approximately 7 MPa, followed by tensile loading until failure occurred. Stress was calculated by dividing the applied load by the measured cross-sectional area of the gauge region, and the peak stress obtained from the stress–strain response was taken as the direct tensile strength. All specimens exhibited cracking within the central gauge region.

The tensile strength of fiber-reinforced UHPC mixtures was determined and compared with UHPC mixtures prepared without and with LP under MC and WB curing conditions. To further investigate the influence of curing, an additional combined curing regimen (WB+MC) was introduced. In this method, specimens were cured as WB curing for the first two days following demolding, after which they were transferred to a MC chamber for the remaining 25 days. This hybrid curing approach was developed to better capture the effect of initial water immersion followed by controlled moisture exposure on the tensile performance of UHPC.

2.3.7. Drying and Autogenous Shrinkage

Two prismatic specimens, each measuring 75 × 75 × 285 mm were cast for each batch, with gauge studs inserted at the ends following ASTM C157 [39], establishing a 250 mm effective length for shrinkage measurement. After casting, the specimens were left in the mold for 24 h before being demolded. Subsequently, they were submerged in lime-saturated water for half an hour prior to taking the initial measurements.

The initial length comparator readings were then recorded. The specimens were then placed in MC regimens for the next two days. After two days of curing, the specimens were left in the air at room temperature for the next 52 days. Length comparator readings were recorded every other day. The method for measuring autogenous shrinkage is similar to that of drying shrinkage with the exception that the specimens were covered with

food-grade plastic wrap/aluminum foil after being saturated in lime water for 30 min to minimize the change in length due to change in temperature.

The value of shrinkage recorded on the 56th day is considered as the ultimate shrinkage for the UHPC mixtures. The average of two samples was reported as the final shrinkage strain which was calculated using Equation (1).

$$\Delta = (L_x - L_0)/10 \quad (1)$$

where L_x represents the length (mm) comparator reading on the test date and L_0 (mm) is the initial length comparator reading.

2.3.8. Rapid Chloride Permeability Test (RCPT)

An RCPT test was conducted according to the ASTM C1202 standard [40] to evaluate the resistance of UHPC to chloride ion ingress. Disk specimens with 100 mm diameter and 50 mm thickness were used. After 28 days of MC and WB curing, the specimens were vacuum saturated and then placed in test cells as per ASTM C1202 [40]. The average charge passed values were reported for the UHPC mixture. ASTM C1202 [40] provides qualitative indications of the chloride ion penetrability based on the charge passed in Coulombs through the test specimen.

2.3.9. Surface Resistivity

The surface resistivity test (SRT) is a newly developed method used to measure the electrical resistivity of water-saturated concrete in kΩ-cm, which provides information about the concrete's ability to resist the penetration of chloride ions. A test method developed by AASHTO TP95-11 [41] was used to evaluate the chloride transport in UHPC mixtures. This laboratory test method assesses the electrical resistivity of UHPC to quickly determine their ability to resist the penetration of chloride ions.

In this test, cylinder specimens (100 mm diameter with 300 mm height) are prepared and cured under MC regimen for 28 days. The circular surface of each sample is marked at four points along its circumference, representing 0, 90, 180, and 270 degrees. A Four-Point Wenner Array Probe is used to determine the electrical resistivity values at 0, 90, 180, and 270 degrees. The average of these electrical resistivity values is then reported. Based on the average value, the amount of chloride ion penetration is evaluated by comparing the values given in AASHTO TP95-11 [41].

2.3.10. Freezing and Thawing

ASTM C 666 [42] assesses concrete's resistance to freezing and thawing by subjecting specimens to rapid, repeated freeze–thaw cycles under controlled laboratory conditions. In this study, molded beam specimens measuring 75 × 100 × 405 mm were cured for 14 days prior to testing. After curing, the specimens underwent a 24-h conditioning period in water maintained at 4 °C. They were then exposed to freeze–thaw cycles, each lasting 3 h and 26 min, consisting of 2 h and 10 min of freezing, 56 min of thawing, and a 10-min soaking period between phases. At intervals of no more than 30 cycles, the specimens were removed from the freezing chamber during the thaw phase to measure their dynamic elastic modulus. Fundamental transverse frequency (for modulus calculations) and mass were recorded throughout testing. The procedure continued until each beam completed at least 300 cycles or its dynamic elastic modulus fell to 90% or less of its initial value. Based on these data, the relative dynamic modulus P_c and durability factor were calculated using Equations (2) and (3).

$$P_c = \left(\frac{n_x}{n_i}\right)^2 \times 100 \quad (2)$$

$$\mathrm{DF} = \frac{PN}{M} \tag{3}$$

where n_x and n_i are the transverse fundamental frequencies at the xth cycle and initial fundamental frequency, respectively. N is the cycle when the relative dynamic modulus falls below 90% and M is the cycle when the test is supposed to be stopped (300 cycles).

3. Results and Discussion

3.1. Workability

The effect of LP on the flowability of both plain and fiber-reinforced UHPC mixtures was evaluated, with results shown in Figure 3. LP incorporation significantly enhanced workability in both cases. In plain UHPC mixtures, replacing 20% of cement with LP increased flow by 14.3%, while in fiber-reinforced mixtures, the same replacement improved workability by 33%. This improvement is attributed to the plasticizing effect of LP [17], which facilitates better particle dispersion. The higher percentage increase in flow observed in the fiber-reinforced UHPC compared with the plain mixture can be attributed to the combined effects of fiber dispersion dynamics and the filler characteristics of LP. In UHPC without LP, the presence of steel fibers tends to hinder flow because fibers create mechanical interlocking and increase internal friction within the mix [43–45]. When LP is introduced, its fine, inert particles enhance particle packing and lubrication of the mix through a micro-ball-bearing effect, reducing frictional resistance between fibers and the surrounding matrix [17,23]. This rheological improvement is particularly pronounced in fiber-reinforced systems, where fiber–matrix and fiber–fiber interactions dominate the flow response and amplify the beneficial influence of LP on workability [46]. Consequently, LP mitigates the typical flow loss caused by fiber addition and results in a proportionally larger improvement in workability for fiber-reinforced UHPC. Similar findings have been reported in studies on LP-modified UHPC and self-consolidating concrete containing steel or synthetic fibers [17,23,47].

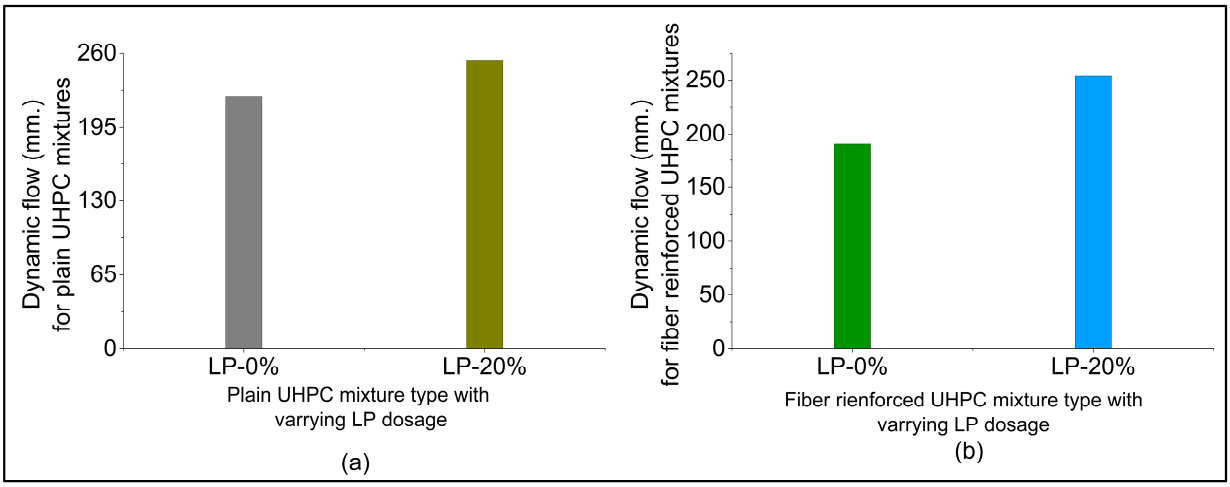


Figure 3. Workability for (**a**) plain and (**b**) fiber-reinforced -UHPC mixture with and without 20% LP.

3.2. Compressive Strength

The average compressive strengths of 50 mm cubes cured under MC and WB regimens for 7, 28, and 56 days for both plain and fiber-reinforced UHPC mixtures with and without LP are presented in Figure 4.

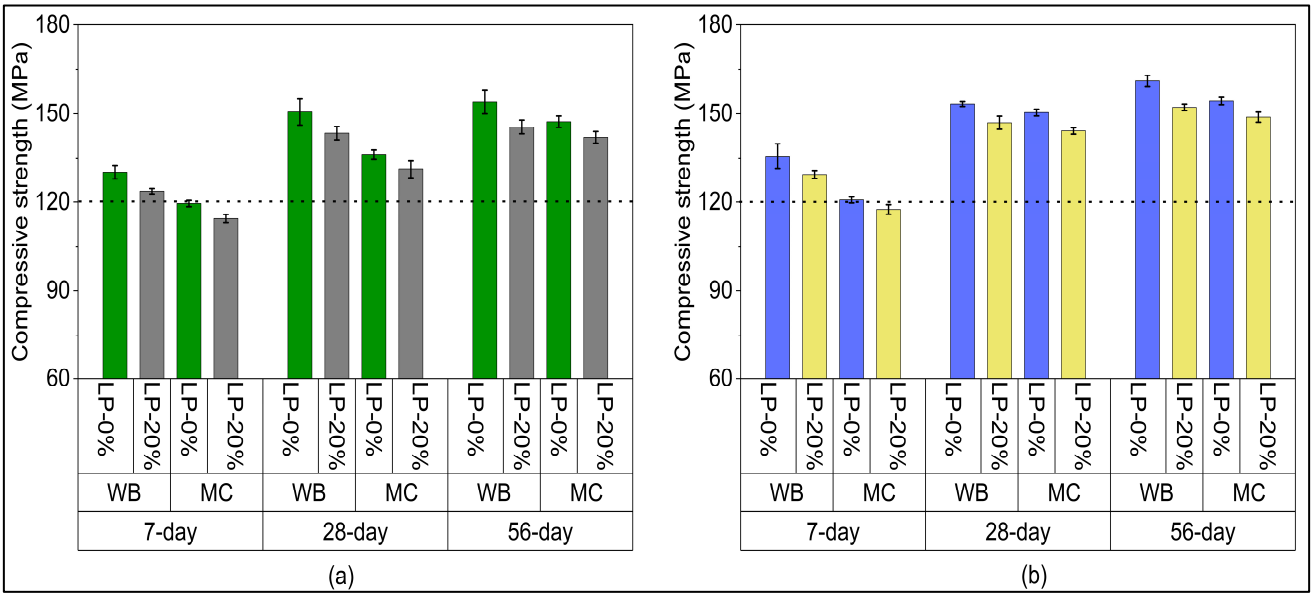


Figure 4. Compressive strength of 50 mm (2-inch) cube for (**a**) plain and (**b**) fiber-reinforced UHPC mixture without GGBFS. The control mixture contains 0% LP and is compared with 20% LP used as cement replacement cured under WB and MC regimens for 7, 28 and 56 days.

For the WB curing regimen at 56 days, the plain UHPC mixture without LP achieved the highest compressive strength of 154 MPa, while the fiber-reinforced mixture without LP reached 161 MPa. In mixtures with 20% LP as a cement replacement, the highest compressive strengths under MC were 142 MPa for plain UHPC and 149 MPa for fiber-reinforced UHPC. Under WB curing, the corresponding values were 145.2 MPa and 152.0 MPa, respectively. Compared to mixtures without LP, plain UHPC mixtures with 20% LP exhibited reductions in compressive strength of 4.15%, 3.59%, and 3.65% after 7, 28, and 56 days of MC, respectively. Similarly, for fiber-reinforced UHPC mixtures with 20% LP, compressive strength decreased by 2.57%, 4.22%, and 3.16% after 7, 28, and 56 days of MC, respectively, compared to mixtures without LP.

Under the WB curing regimen, the compressive strength of plain UHPC mixtures with 20% LP as a cement replacement decreased by 2.71%, 2.12%, and 4.05% after 7, 28, and 56 days, respectively, compared to mixtures without LP. For fiber-reinforced UHPC mixtures, the reductions were 2.79%, 4.22%, and 5.52% over the same time periods. The decrease in compressive strength is attributed to LP's lack of pozzolanic reactivity with cement [48], which prevents the formation of additional C–S–H gel [21,48]. Furthermore, replacing cement with LP in the UHPC matrix contributes to strength loss through physical mechanisms such as the dilution effect and the filler effect [26,49].

As shown in Figure 4, higher curing temperatures and longer curing periods improved the compressive strengths of both plain and fiber-reinforced UHPC mixtures, regardless of LP content. This enhancement is attributed to accelerated hydration at elevated temperatures, which increases the formation of hydration products [50,51].

Figure 5a,b show compressive strengths achieved at 7 and 56 days, using the 28-day strength as the baseline (100%).

Under MC, plain UHPC mixtures without and with 20% LP reached 87.70% and 87.27% of their 28-day strength at 7 days, increasing by 8.16% and 8.09% by 56 days. Fiber-reinforced mixtures achieved 80.22% and 81.60% in 7 days, increasing by 2.66% and 3.30% by 56 days.

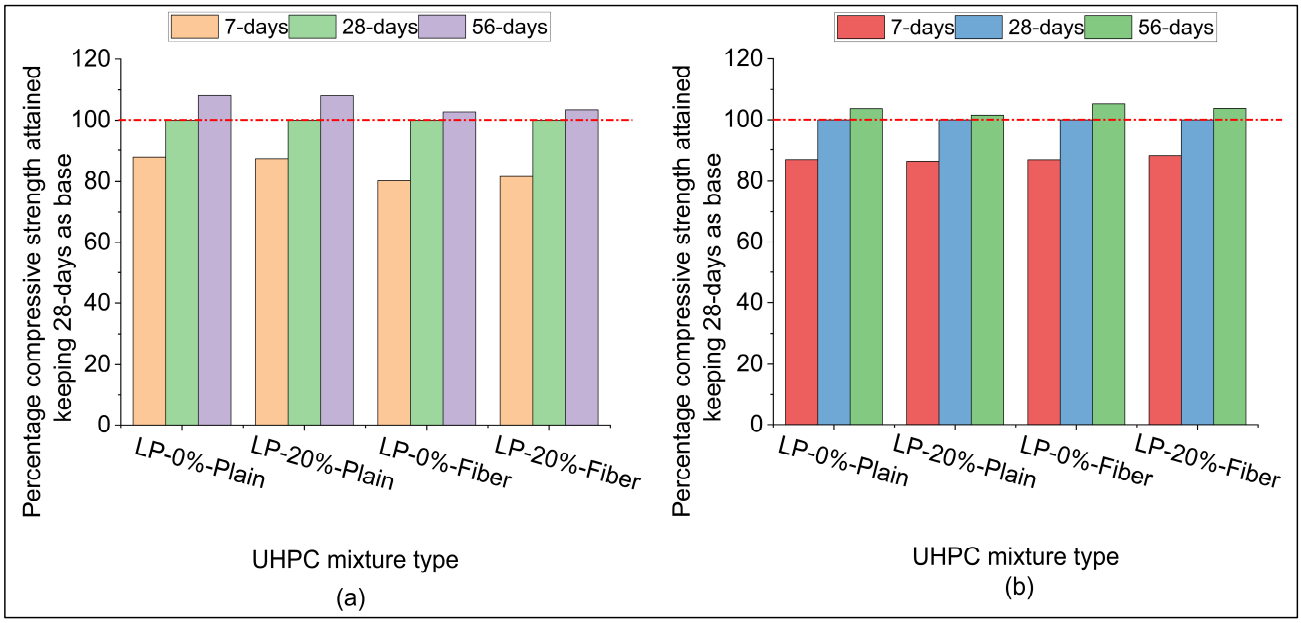


Figure 5. Percentage compressive strength attained after 7 and 56 days under (**a**) MC and (**b**) WB curing, expressed relative to the 28-day strength (baseline = 100%). The red line represents the 28-day reference strength.

Under WB curing, plain UHPC mixtures without and with LP reached 86.80% and 86.27% at 7 days, increasing by 3.53% and 1.49% by 56 days. Fiber-reinforced mixtures reached 86.77% and 88.06% at 7 days, increasing by 5.03% and 3.61% by 56 days.

Statistical analysis confirmed that the compressive strengths of mixtures with 20% LP were significantly different ($p < 0.05$) from those without LP in both plain and fiber-reinforced UHPC. Nevertheless, all mixtures exceeded 120 MPa after 28 days under both curing regimes, meeting the standard UHPC strength [52].

3.3. Split Tensile Strength

The splitting tensile strengths of plain and fiber-reinforced UHPC mixtures, with and without 20% LP as a cement replacement, were evaluated after 7 and 28 days under MC and WB curing regimens (Figure 6). For mixtures without LP, the highest strengths were 7.2 MPa for plain UHPC and 12.1 MPa for fiber-reinforced UHPC, both achieved under WB curing at 28 days. Under the same conditions, mixtures with 20% LP reached 5.9 MPa (plain) and 11.3 MPa (fiber-reinforced). For plain UHPC with 20% LP under MC, splitting tensile strength decreased by 15.38% at 7 days and 13.33% at 28 days compared to mixtures without LP. For fiber-reinforced UHPC under MC, reductions were 9.45% and 5.88% at the same ages. Under WB curing, plain UHPC with 20% LP showed decreases of 20.72% and 18.66% at 7 and 28 days, respectively, while fiber-reinforced UHPC showed reductions of 11.00% and 7.10%. The mechanical performance of UHPC is closely linked to its microstructure [53]. LP replacement affects hydration product formation, increasing porosity and weakening the interfacial transition zone (ITZ) and matrix bonding strength [54,55]. Increasing LP replacement tends to minimize the formation of hydration products, resulting in greater porosity. This affects the ITZ and bonding strength of the concrete matrix [55]. Similar trends have been reported by Demirhan et al. [56], who found that LP contents above 15% did not improve splitting tensile strength across curing periods.

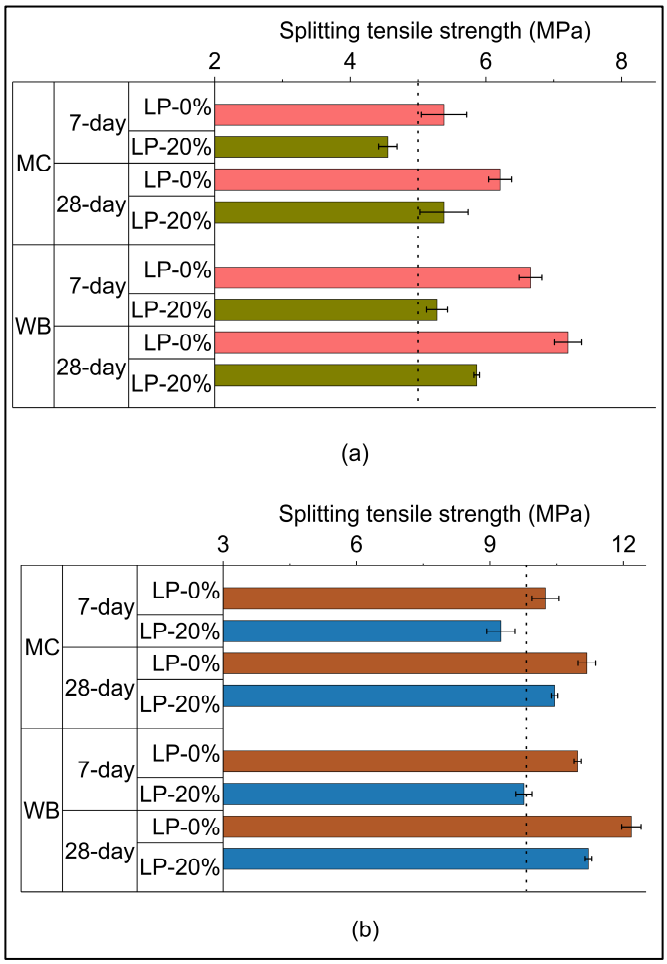


Figure 6. Splitting tensile strength of 100 mm × 200 mm cylinders for (**a**) plain and (**b**) fiber UHPC mixture without GGBFS. The control mixture contains 0% LP and is compared with 20% LP used as cement replacement cured under WB and MC regimens for 7 and 28 days.

Statistical analysis confirmed a significant reduction ($p < 0.05$) in splitting tensile strength with 20% LP compared to mixtures without LP, for both plain and fiber-reinforced UHPC. However, even with this reduction, 20% LP mixtures exceeded the typical UHPC benchmarks of 5 MPa for plain UHPC and 10 MPa for fiber-reinforced UHPC under WB curing after 28 days.

3.4. Modulus of Elasticity (MOE)

Figure 7 presents the MOE values for plain and fiber-reinforced UHPC mixtures, with and without 20% LP as a cement replacement. For plain UHPC, the greatest MOE values were 37.0 GPa (without LP) and 36.1 GPa (with LP) under MC, and 40.6 GPa (without LP) and 36.9 GPa (with LP) under WB curing.

For fiber-reinforced UHPC, the highest MOE values were 44.6 GPa (without LP) and 38.6 GPa (with LP) under MC, and 50.0 GPa (without LP) and 42.5 GPa (with LP) under WB curing.

Since MOE and compressive strength are correlated, both elevated curing temperature and steel fiber addition improved these properties. However, replacing cement with 20% LP reduced MOE for all mixtures. Compared to mixtures without LP, MOE decreased by 2.23% (MC) and 8.15% (WB) for plain UHPC, and by 13.31% (MC) and 14.66% (WB) for fiber-reinforced UHPC. This reduction trend mirrors that observed for compressive strength.

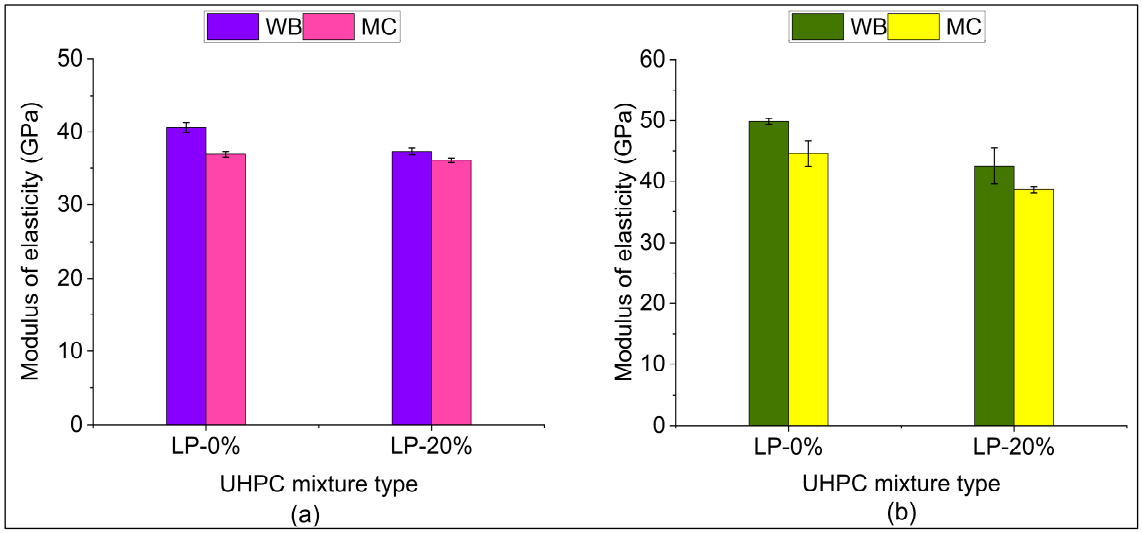


Figure 7. Modulus of elasticity of the UHPC mixtures, without and with 20% LP under different curing regimens. (**a**) the modulus of elasticity of plain UHPC mixtures and (**b**) the modulus of elasticity of fiber-reinforced UHPC mixtures.

3.5. Flexural Properties

Load–deflection curves were obtained following ASTM C1609 [37] and are shown in Figure 8. A typical curve for fiber-reinforced UHPC consists of three distinct stages. Stage I (red arrow) represents the linear-elastic region up to the first crack, where load increases proportionally with deflection. Stage II (black arrow) is the strain-hardening region, characterized by distributed microcracking and increased fiber contribution, leading to the peak load. Stage III (blue arrow) represents the softening phase and crack localization.

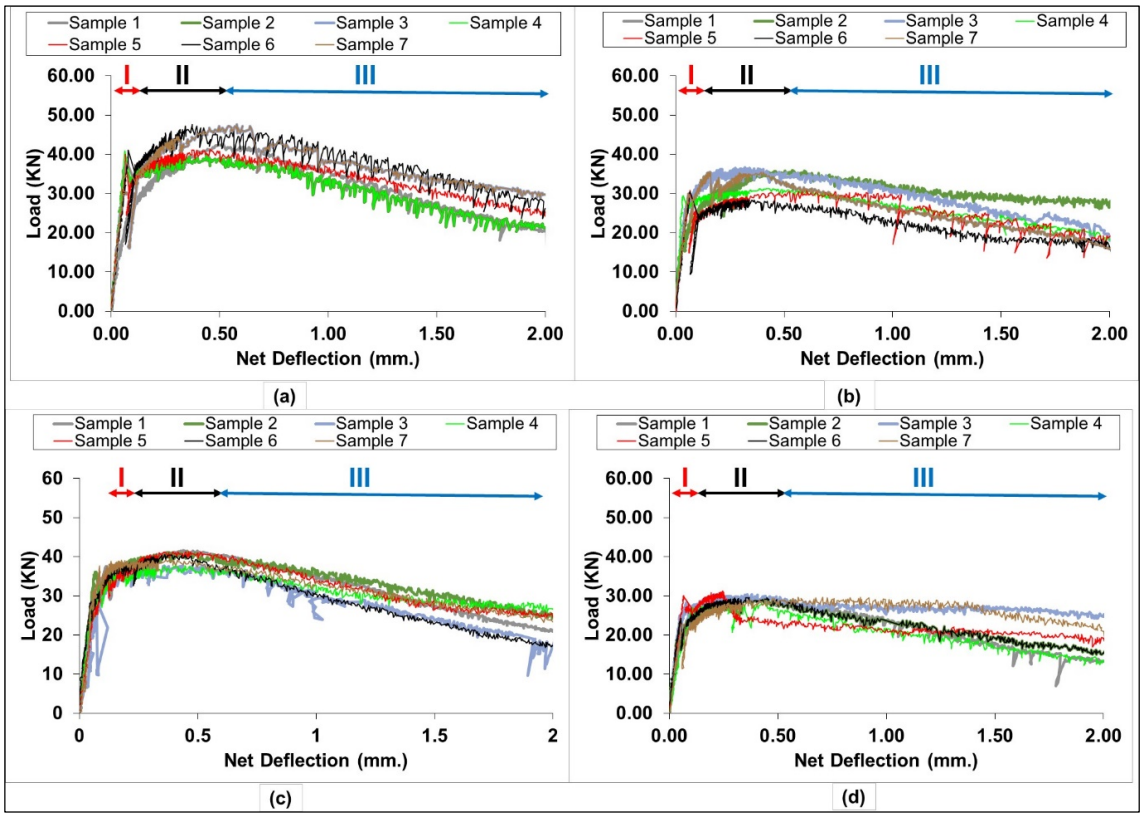


Figure 8. Load–deflection curves for fiber-reinforced UHPC mixtures: (**a**) without LP, MC; (**b**) with 20% LP, MC; (**c**) without LP, WB curing; (**d**) with 20% LP, WB curing.

Zang et al. [57] further discussed the inelastic stages, stage I and stage II, where steel fibers contribute. These are:

- Transition stage (I): Load-bearing capacity decreases as tensile stresses transfer from the concrete matrix to the steel fibers, initiating micro-cracks.
- Deflection hardening stage (II): Load continues to increase with deflection as fibers bridge cracks and hinder propagation.
- Post-peak stage (III): Significant ductility is observed, with load capacity gradually decreasing due to bond failure or fiber rupture.

From the load–deflection curves (Figure 8), key performance indicators were determined for all UHPC mixtures: first-crack strength (modulus of rupture, MOR), peak strength, residual strengths at L/150 and L/600, and toughness. Figure 9 presents the average MOR for fiber-reinforced UHPC mixtures with and without 20% LP after 28 days under MC and WB curing.

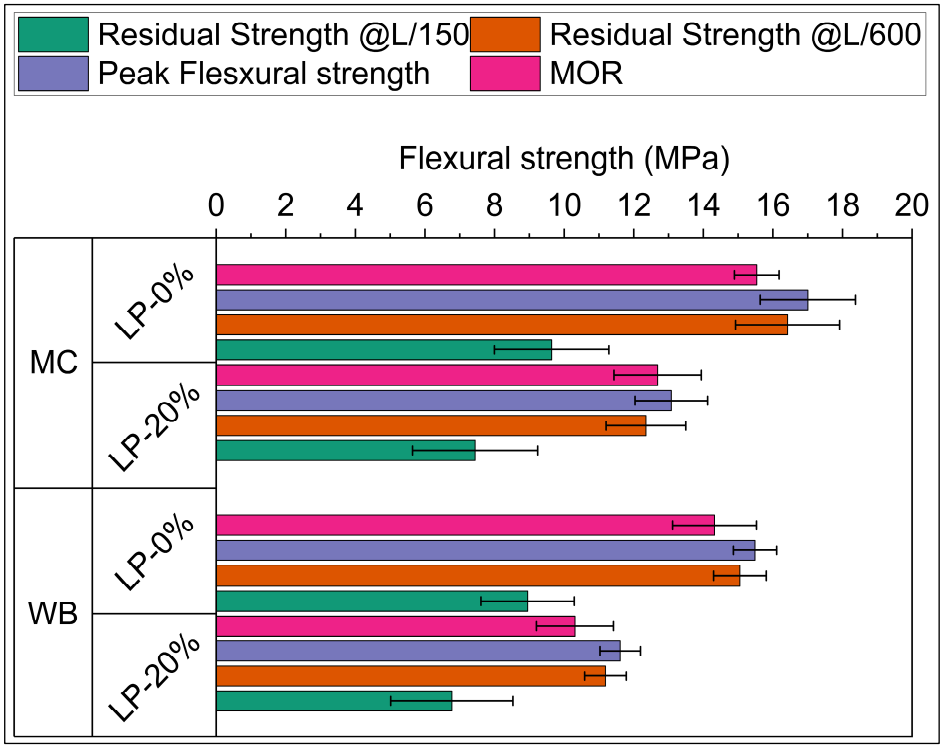


Figure 9. Average MOR for fiber-reinforced UHPC mixtures, with and without 20% LP at 28 days under MC and WB curing regimens.

Overall, flexural strengths were higher under MC compared to WB curing, which contrasts with the compressive strength trend. This reversal may be due to larger specimen size, making them more sensitive to steep temperature gradients during heat curing, as reported by Hu et al. [58]. Tautanji et al. [59] similarly noted that silica fume addition can promote micro-shrinkage cracking, further influencing flexural performance. Consequently, curing appears to have a greater effect on flexural strength than on compressive strength.

3.5.1. Modulus of Rupture

Figure 9 presents the first-cracking strength (MOR) values for fiber-reinforced UHPC mixtures. Without LP, MOR values were 15.5 MPa (MC) and 14.3 MPa (WB curing). With 20% LP as a cement replacement, MOR decreased to 12.7 MPa (MC) and 10.3 MPa (WB).

This corresponds to reductions of 18.1% under MC and 28.0% under WB curing. The reduction in MOR with increasing LP content parallels the compressive strength trend, and

is primarily attributed to the dilution effect, where LP does not participate in pozzolanic reactions and reduces the volume of hydration products [60].

Statistical analysis confirmed that, at the 5% significance level, MOR values for UHPC mixtures with 20% LP were significantly lower than those without LP under both MC and WB curing.

3.5.2. Peak Flexural Strength

From the load–deflection curves (Figure 8), it is evident that after first cracking, the beams retained substantial load-carrying capacity due to the bridging action of steel fibers, underscoring the importance of peak flexural strength. Figure 10 shows the peak flexural strength values. For fiber-reinforced UHPC mixtures without LP, peak strengths were 17.0 MPa (MC) and 15.5 MPa (WB curing). With 20% LP as a cement replacement, these values decreased to 13.1 MPa (MC) and 11.6 MPa (WB), representing reductions of 23.09% and 25.04%, respectively. Statistical analysis at the 5% significance level confirmed that the peak flexural strength of mixtures with 20% LP was significantly lower ($p < 0.05$) than that of mixtures without LP under both curing conditions.

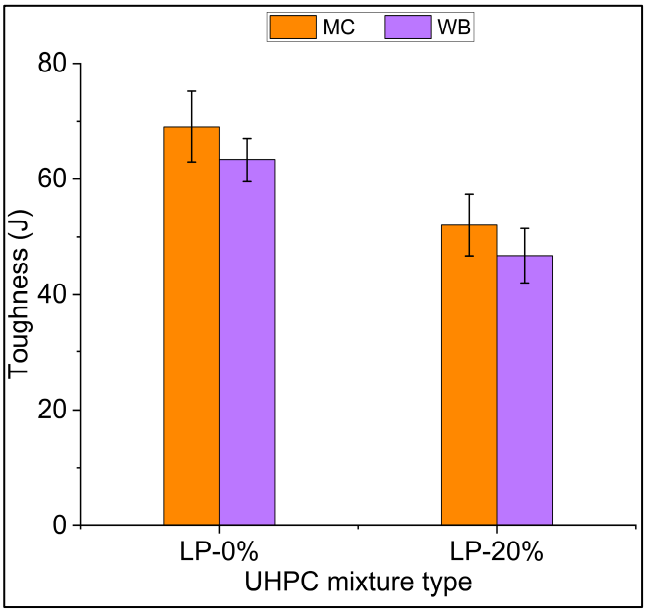


Figure 10. Average 28-day toughness values of fiber-reinforced UHPC mixtures with and without 20% LP as cement replacement, under MC and WB curing regimens.

3.5.3. Residual Flexural Strength

Residual flexural strength, derived from the load–deflection curves (Figure 8), is a key indicator of the post-cracking performance of UHPC mixtures. Figure 9 presents residual strengths at net deflections of 0.50 mm and 2.03 mm.

At 0.50 mm deflection, the highest residual strength was 16.4 MPa for fiber-reinforced UHPC mixtures without LP and 12.3 MPa for mixtures with 20% LP, both under MC. For mixtures with 20% LP, residual strengths were 12.3 MPa (MC) and 11.1 MPa (WB curing), representing reductions of 16.63% and 15.63%, respectively, compared to mixtures without LP.

At 2.03 mm deflection, the highest residual strength was 9.6 MPa for mixtures without LP and 7.4 MPa for mixtures with 20% LP under MC. For mixtures with 20% LP, residual strengths were 9.6 MPa (MC) and 8.9 MPa (WB curing), corresponding to decreases of 22.83% and 24.36%, respectively, relative to mixtures without LP.

Statistical analysis confirmed that, at the 5% significance level, residual flexural strengths at both 0.50 mm and 2.03 mm deflections were significantly lower ($p < 0.05$) for mixtures containing 20% LP compared to those without LP.

3.5.4. Toughness

Toughness, representing the energy absorption capacity prior to failure, was calculated from the area under the load–deflection curve (Figure 8) at a net deflection of L/150. Figure 10 shows the 28-day toughness values for fiber-reinforced UHPC mixtures with and without 20% LP. For mixtures without LP, the highest toughness was 67.8 J under MC, while with 20% LP, the maximum value was 63.7 J under MC. WB curing produced lower toughness values for all mixtures compared to MC.

The addition of 20% LP reduced toughness in all cases. Under MC, toughness decreased from 74.4 J (without LP) to 51.11 J (with LP), a reduction of 31.37%. Under WB curing, toughness declined from 63.2 J (without LP) to 45.9 J (with LP), representing a 27.41% reduction. This reduction indicates a decrease in post-cracking energy absorption and a slightly reduced capacity of the UHPC matrix to bridge and redistribute stresses after cracking. This suggests a marginal weakening of the fiber–matrix interaction within the cementitious paste, likely due to the dilution of hydration products and changes in the interfacial microstructure. Similar trends have been reported in other UHPC systems containing mineral fillers or supplementary cementitious materials, where partial binder replacement modifies the fiber–matrix bond and lowers overall fracture energy [61,62]. While the toughness loss implies a lower resistance to crack propagation under service loads, the measured values remain within the typical range reported for fiber-reinforced UHPC, indicating that overall ductility and load-carrying capacity are largely preserved when adequate fiber content and distribution are maintained. Comparable observations were made by Zhuang et al. [24] and Meng and Khayat [47], who found that although LP and other SCMs slightly reduced toughness and energy absorption, the dense microstructure of UHPC and fiber bridging mechanisms maintained overall ductility and crack control in UHPC. Statistical analysis confirmed that, at the 5% significance level, the toughness values for mixtures with 20% LP were significantly lower ($p < 0.05$) than those without LP for both curing regimens.

3.5.5. Equivalent Flexural Strength Ratio

The equivalent flexural strength ratio was evaluated to assess the post-cracking performance of the developed UHPC mixtures. This ratio quantifies the percentage of peak flexural strength retained at a specific deflection point and is calculated following the methods outlined by Nayyar et al. [63], Rashiddadash et al. [64] and Liu et al. [65], in accordance with ASTM C1609 [37] (Equation (4)):

$$R^D_{Tn} = \frac{nT^D_n}{f_P bh^2} \quad (4)$$

where

n is deflection ratio corresponding to the toughness measurement (e.g., 150 at the deflection of L/150).

T^D_n is toughness measured at the deflection of L = n in N/mm.

f_P is peak flexural strength in N/mm^2.

b and h are cross-sectional dimensions of the flexural specimen in mm.

Figure 11 presents the equivalent flexural strength ratios for all fiber-reinforced UHPC mixtures at net deflections of L/600 and L/150. For example, for the fiber-reinforced UHPC mixture without LP under MC, the ratio was 76.93% at L/150, indicating that this

proportion of peak flexural strength was maintained at the specified deflection. At L/600, the same mixture achieved an equivalent flexural strength ratio of 81.62%. Across all fiber-reinforced UHPC mixtures, the equivalent flexural strength ratio ranged from 80–86% at L/600 and 75–77% at L/150. These results indicate that the inclusion of 20% LP as a cement replacement had no significant effect on post-cracking performance under either MC or WB curing conditions.

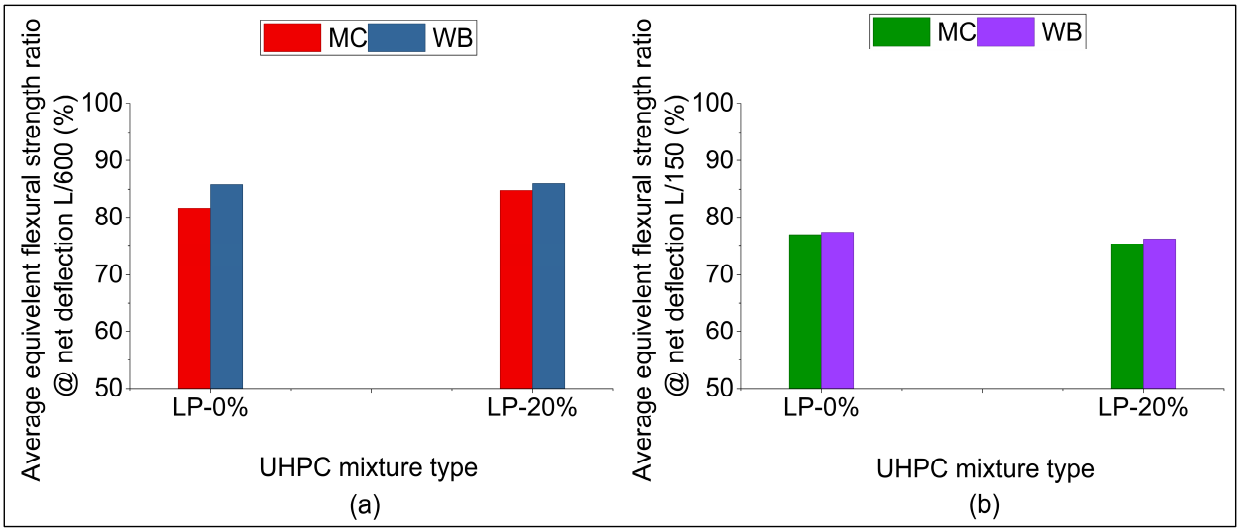


Figure 11. Average equivalent flexural strength ratios for fiber-reinforced UHPC mixtures without and with 20% LP: (**a**) at net deflection L/600 and (**b**) at net deflection L/150.

3.6. Direct Tensile Strength

The tensile strength of the proposed fiber-reinforced UHPC mixtures was compared with baseline mixtures without LP. Stress–strain curves were plotted to determine the peak stress values, which were reported as the direct tensile strength. Graybeal et al. [38] described the ideal tensile mechanism in three regions: R1, the elastic region up to the first crack, R2, the cracking region with distributed microcracks; and R3, the crack localization region with significant crack widening. These regions are illustrated in Figure 12 for specimens subjected to WB, MC, and combined MC+WB curing regimens.

The combined MC+WB regimen was included to examine the effect of sequential curing on tensile performance, as elevated curing temperatures can induce thermal cracking, potentially reducing tensile strength. To mitigate thermal shock in the combined curing regimen, specimens cured in a WB at elevated temperatures were allowed to cool while submerged before being transferred to the MC chamber.

Results in Figure 13 indicate that all UHPC mixtures achieved tensile strengths exceeding the 5 MPa minimum required for classification as UHPC. The average 28-day tensile strengths for fiber-reinforced UHPC mixtures with 20% LP were: 8.6 MPa under WB curing, 7.6 MPa under MC+WB curing, and 6.7 MPa under MC. Compared to corresponding mixtures without LP, these strengths were reduced by 14.50%, 6.00%, and 13.15%, respectively. The greatest tensile strength values were observed under WB curing, which can be attributed to the improvement of the interfacial transition zone (ITZ) at elevated temperatures, enhancing fiber–matrix bonding [66,67]. The MC+WB curing regimen also improved tensile strength compared to MC alone, as initial elevated curing enhanced microstructural development, resulting in early-age strength gains.

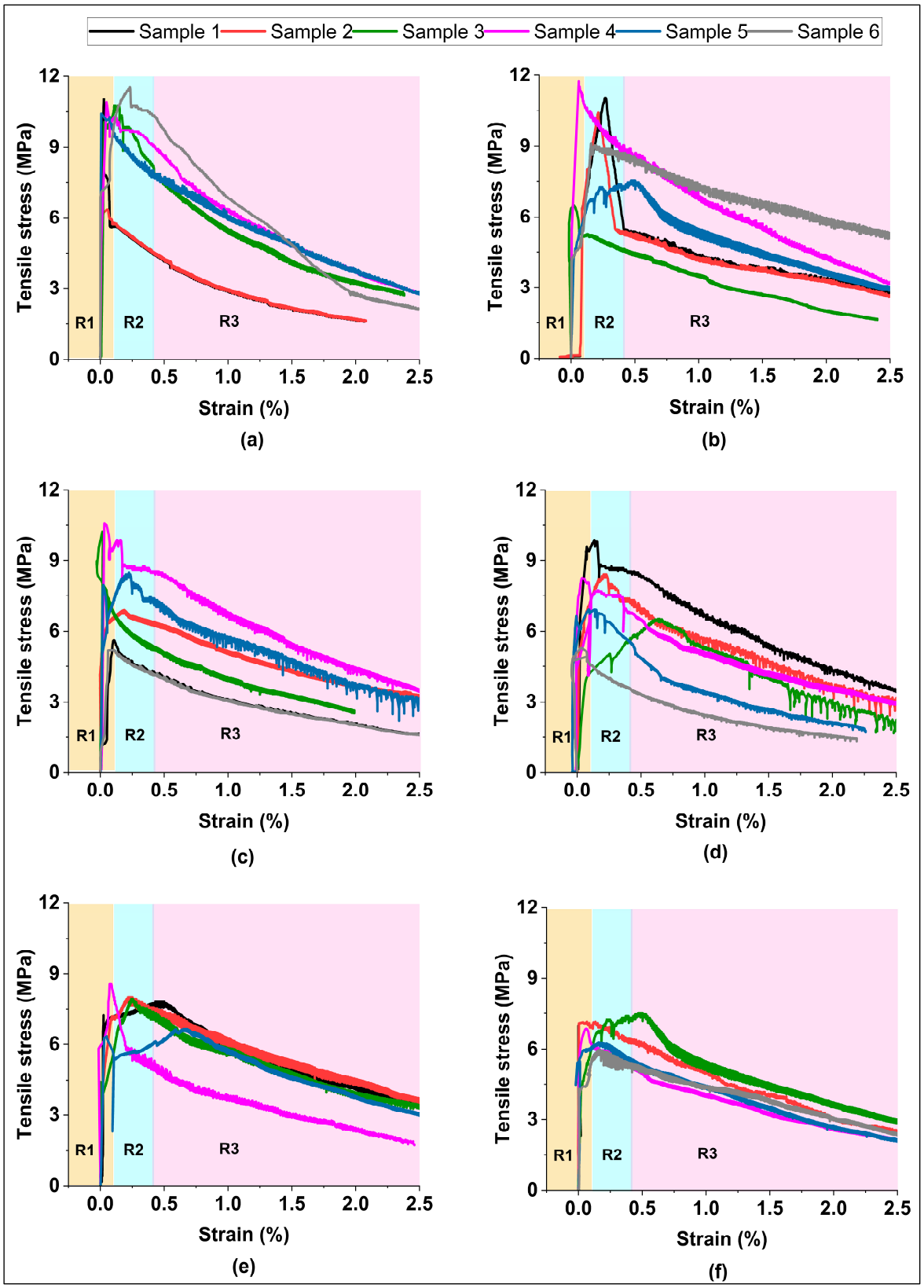


Figure 12. Tensile stress–strain curves for fiber-reinforced UHPC mixtures: (**a**) without LP, WB curing; (**b**) with 20% LP, WB curing; (**c**) without LP, MC+WB curing; (**d**) with 20% LP, MC+WB curing; (**e**) without LP, MC; and (**f**) with 20% LP, MC.

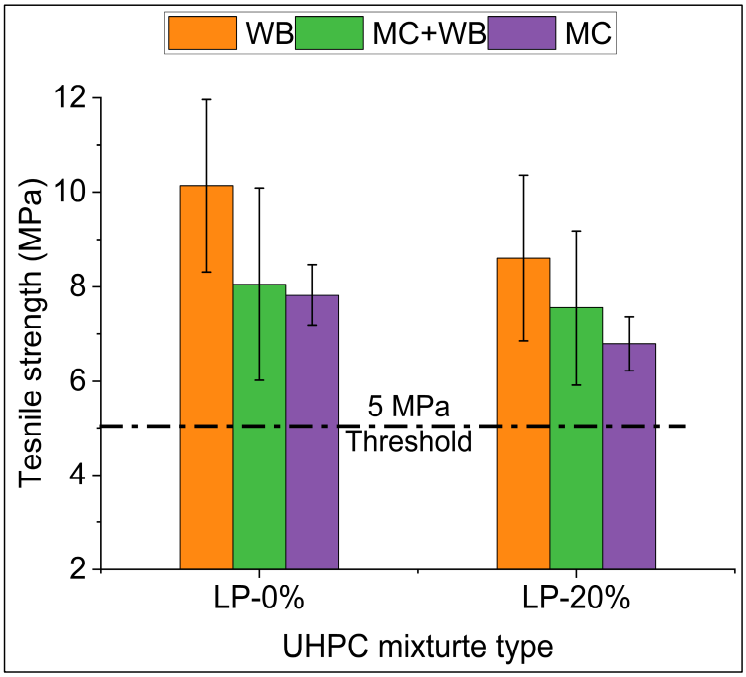


Figure 13. Average tensile strength of fiber-reinforced UHPC mixtures with 0% and 20% LP, cured under MC, MC+WB, and WB regimens.

However, the inclusion of LP as a cement replacement reduced tensile strength due to the dilution effect, where a less reactive or non-reactive material replaces cement, producing fewer hydration products and consequently weakening the matrix [68]. Statistical analysis at a 5% significance level indicated no significant difference in tensile strength between UHPC mixtures with and without 20% LP under WB and MC. The only significant difference was observed for specimens cured under the MC+WB regimen.

3.7. Shrinkage

3.7.1. Autogenous Shrinkage

The average autogenous shrinkage values for all UHPC mixtures are shown in Figure 14. The plain UHPC mixture without LP exhibited an average autogenous shrinkage of 672 με, while the plain mixture with 20% LP showed 468 με. For fiber-reinforced UHPC, the corresponding values were 566 με without LP and 408 με with LP.

As seen in Figure 15, a distinct transition or "knee point" occurred between the fourth and seventh days for plain UHPC mixtures with and without LP. For fiber-reinforced mixtures, the knee point appeared on the fourth day in both cases. This transition marks a period of rapid volumetric change, which can influence early-age cracking potential and long-term durability [69,70].

Fiber-reinforced UHPC mixtures consistently showed lower autogenous shrinkage than plain mixtures. Without LP, fiber-reinforced mixtures had a 15.47% reduction compared to plain UHPC; with 20% LP, the reduction was 7.40%. The high elasticity of steel fibers helps restrict crack widths and limits crack propagation during autogenous shrinkage [71].

Comparing mixtures with and without LP, 20% LP replacement reduced autogenous shrinkage by 35.6% for plain UHPC and by 29.4% for fiber-reinforced UHPC. Previous studies by Li et al. [17] and Yang et al. [27] reported similar trends, attributing the reduction to the slower hydration process and lower formation of hydration products when LP is used as a cement replacement. Statistical analysis confirmed that, at the 5% significance level,

autogenous shrinkage values differed significantly between mixtures with and without LP for both plain and fiber-reinforced UHPC.

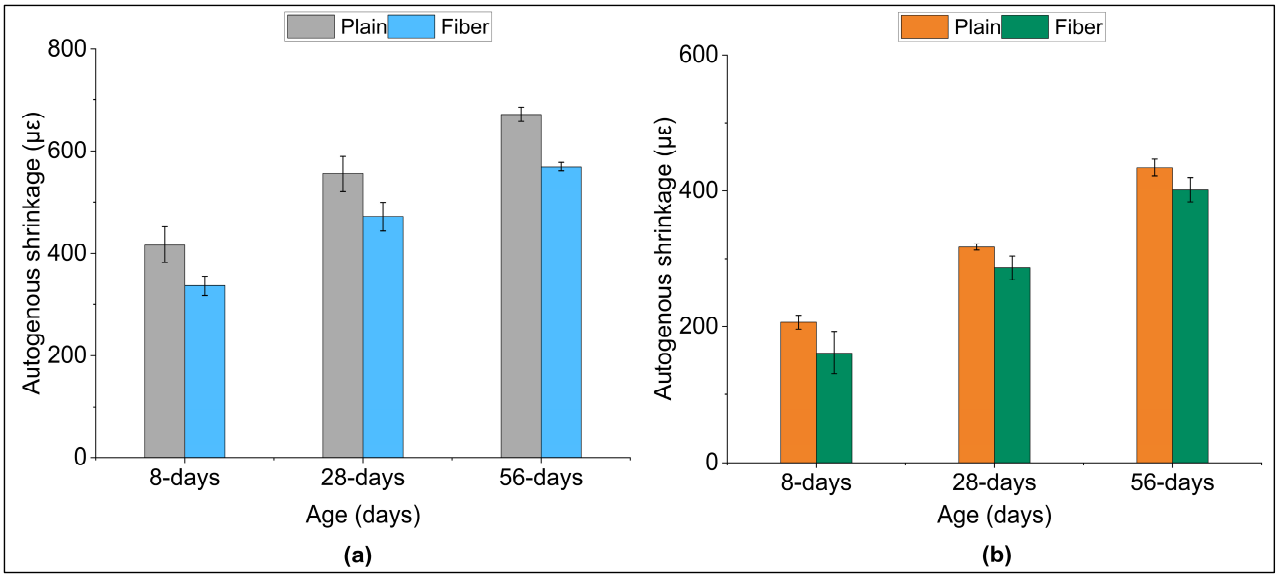


Figure 14. Average autogenous shrinkage values for (**a**) plain and fiber-reinforced UHPC mixtures without LP, and (**b**) plain and fiber-reinforced UHPC mixtures with 20% LP at 8, 28, and 56 days. Approximately half of the total autogenous shrinkage occurs within the first eight days.

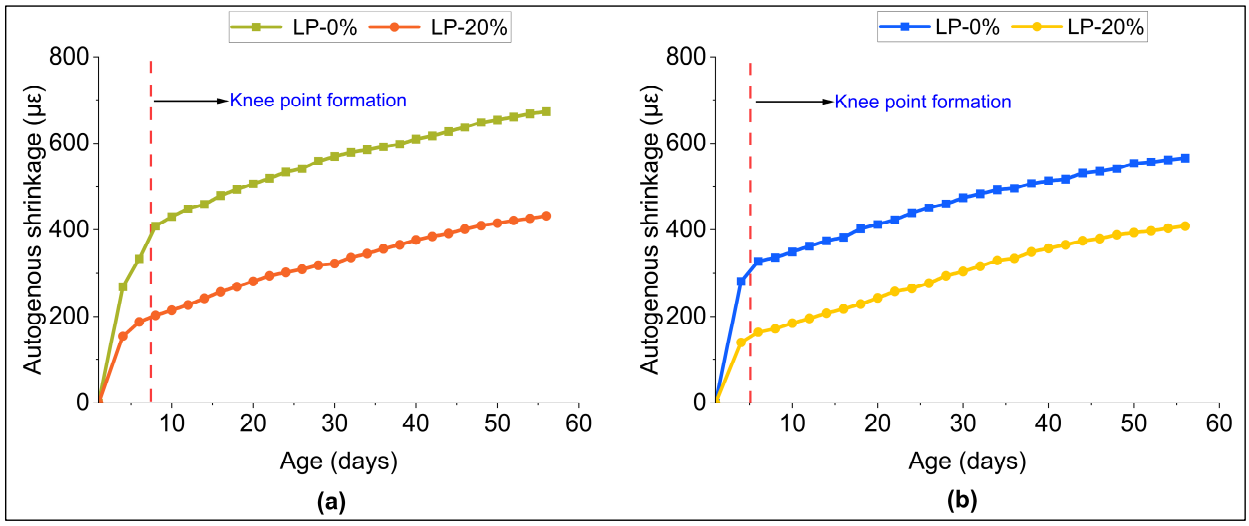


Figure 15. Average autogenous shrinkage values for (**a**) plain UHPC mixtures and (**b**) fiber-reinforced UHPC mixtures, both without and with 20% LP. The "knee point," indicating a rapid volumetric change, occurs between the 4th and 7th days for plain mixtures and on the 4th day for fiber-reinforced mixtures.

3.7.2. Drying Shrinkage

The average drying shrinkage values for all UHPC mixtures are illustrated in Figure 16. The plain UHPC mixture without LP exhibited an average drying shrinkage of 696 με, while the plain UHPC mixture with 20% LP recorded 533 με. In contrast, fiber-reinforced UHPC mixtures showed drying shrinkage values of 602 με without LP and 432 με with 20% LP.

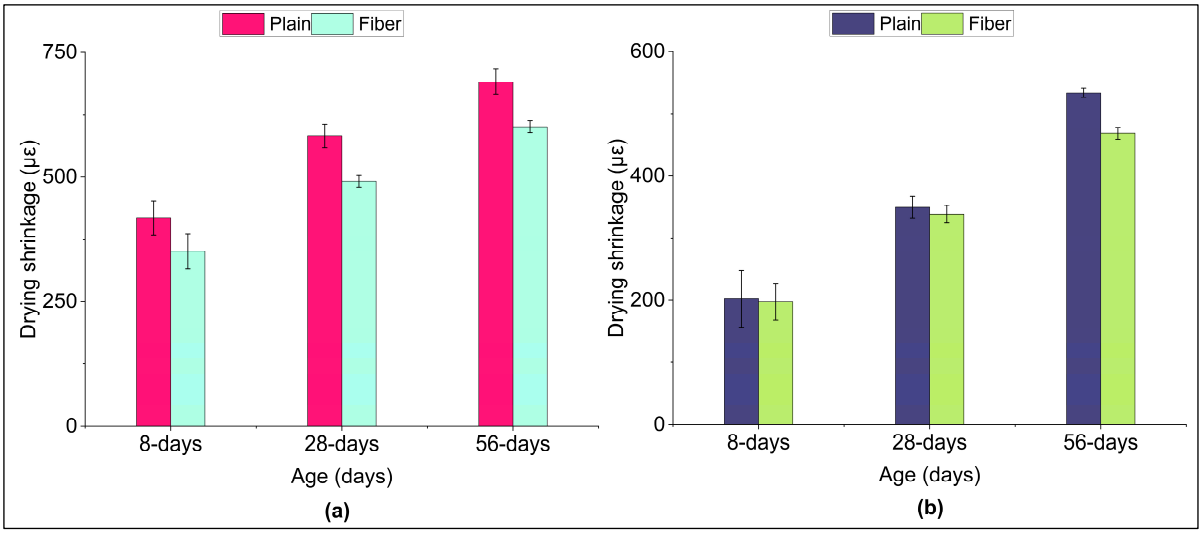


Figure 16. Average drying shrinkage values for (**a**) plain and fiber-reinforced UHPC mixtures without LP and (**b**) plain and fiber-reinforced UHPC mixtures with 20% LP, measured at 8, 28, and 56 days.

From Figure 17, it can be observed that the "knee point"—the critical transition indicating a period of rapid volumetric change—occurred between the 5th and 8th days for plain UHPC mixtures, both with and without LP. For fiber-reinforced mixtures, this knee point was observed on the 4th day for both LP and non-LP mixtures.

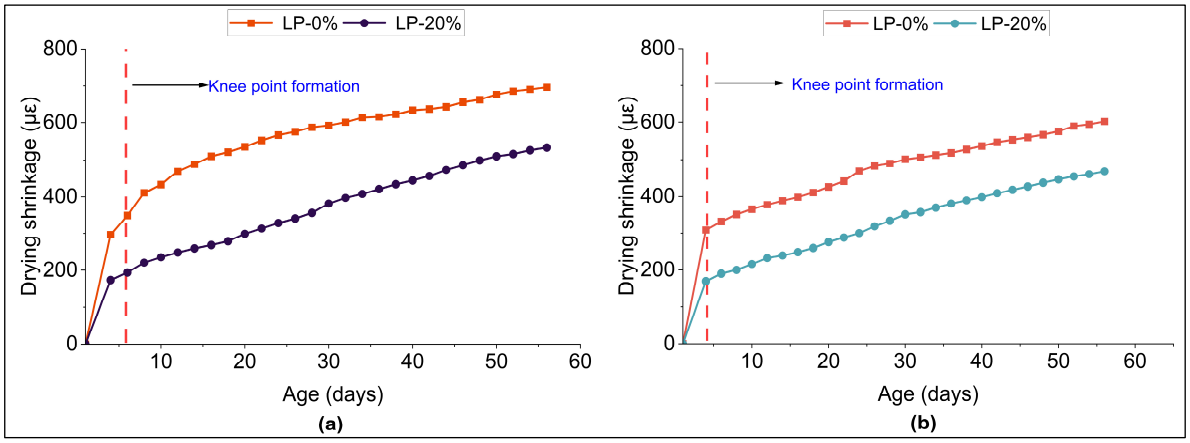


Figure 17. Average drying shrinkage development for (**a**) plain UHPC mixtures without GGBFS and (**b**) fiber-reinforced UHPC mixtures without GGBFS, both with and without 20% LP as a cement replacement, showing the knee point formation period under 56-day monitoring.

The drying shrinkage values for all UHPC mixtures at 8, 28, and 56 days are presented in Figure 16. For plain and fiber-reinforced UHPC mixtures without LP, 60.0% of the total drying shrinkage occurred within the first eight days. With 20% LP replacement, 38.0% and 42.0% of the total drying shrinkage was reached within eight days for plain and fiber-reinforced mixtures, respectively—indicating that approximately half of the total drying shrinkage typically develops during the initial curing period.

Compared to plain UHPC mixtures, fiber-reinforced UHPC mixtures exhibited lower drying shrinkage for both LP and non-LP formulations. Specifically, fiber-reinforced mixtures without LP showed a 13.0% reduction, while those with 20% LP exhibited a 12.2% reduction compared to plain UHPC mixtures. This reduction is attributed to the stress-distribution ability of steel fibers, which mitigates shrinkage-induced microcracking by reducing stress concentrations in the matrix [72].

When comparing UHPC mixtures with 20% LP to those without LP, the drying shrinkage decreased by 23.4% for plain mixtures and by 28.2% for fiber-reinforced mixtures. This is because LP has lower reactivity than cement and other SCMs such as fly ash and silica fume, and functions primarily as an inert filler. By replacing a portion of cement, LP effectively increases the water-to-cement ratio of the reactive binder, which in turn reduces drying shrinkage in UHPC mixtures [73].

Statistical analysis confirmed that, at the 5% significance level, the drying shrinkage differences between LP and non-LP mixtures—both plain and fiber-reinforced—were significant ($p < 0.05$).

3.8. Resistance to Rapid Freezing and Thawing Cycles

The resistance of plain and fiber-reinforced UHPC mixtures, both with and without 20% LP as a cement replacement, was evaluated against rapid freeze–thaw cycles in accordance with ASTM C666 [42]. Figure 18 illustrates the relative dynamic modulus for these mixtures. The relative dynamic modulus of all UHPC mixtures remained essentially constant throughout three hundred cycles of rapid freezing and thawing, regardless of the presence or absence of steel fibers. The specimen mass did not change during the three hundred cycles, indicating that no microcracking occurred due to freeze–thaw exposure. All UHPC mixtures demonstrated a relative dynamic modulus ranging from 100% to 103%.

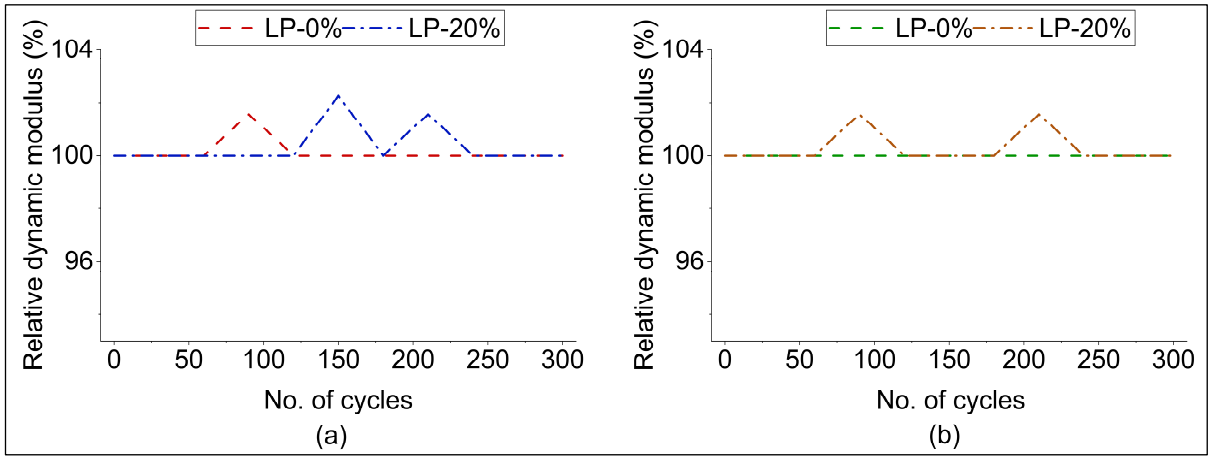


Figure 18. Average relative dynamic modulus from rapid freezing-thawing cycles of (**a**) plain UHPC mixture and (**b**) fiber-reinforced UHPC mixture without and with 20% LP.

MOR values were determined at fourteen days (immediately following MC curing) and after three hundred freeze–thaw cycles.

Figure 19 presents the results for plain and fiber-reinforced UHPC mixtures, respectively. For plain UHPC mixtures (Figure 19a), the MOR decreased by 4.7% for mixtures without LP and by 1.1% for mixtures with 20% LP after three hundred cycles, compared to the fourteen-day MOR values. For fiber-reinforced UHPC mixtures (Figure 19b), the MOR decreased by 8.1% for mixtures without LP and by 3.7% for mixtures with 20% LP after three hundred cycles.

These results demonstrate that incorporating 20% LP as a cement replacement reduced the percentage loss in MOR after three hundred cycles compared to the fourteen-day values. Furthermore, the fourteen-day MOR values of plain UHPC mixtures without LP were 20.0% lower, and those of fiber-reinforced mixtures were 26.1% lower than the respective values of mixtures with 20% LP. After three hundred cycles, the MOR values for mixtures without LP decreased by 17.25% (plain UHPC) and 21.45% (fiber-reinforced UHPC) compared to mixtures with 20% LP.

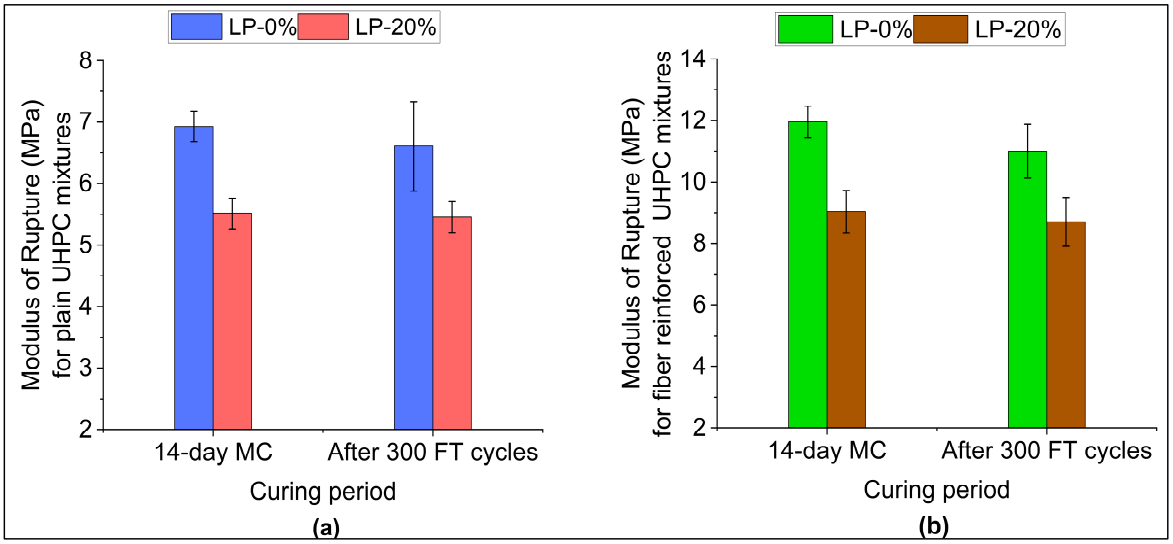


Figure 19. Modulus of rupture values of UHPC mixtures with and without LP for (**a**) plain and (**b**) fiber-reinforced at 14 days of MC and after 300 freeze thaw cycles.

Overall, the addition of LP mitigated the reduction in MOR due to rapid freezing and thawing. Muro-Villanueva et al. [74] reported a 60% loss in flexural strength compared to seven-day MOR values, attributed to enlargement of pore sizes across UHPC specimens subjected to freeze–thaw cycles. According to ASTM C666 [42], a durability factor (DF) above 95% indicates excellent freeze–thaw resistance. The DF for all UHPC mixtures exceeded 100%, confirming outstanding resistance to freeze–thaw damage.

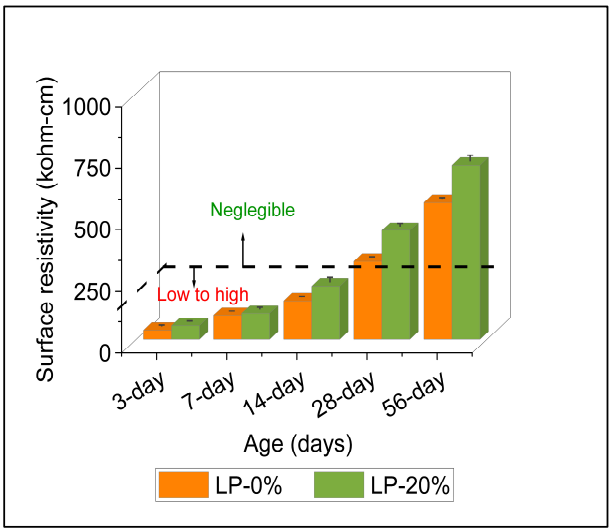
3.9. Surface Resistivity

The surface resistivity (SR) values of all UHPC mixtures were measured at 3, 7, 14, 28, and 56 days for specimens cured under the MC regimen. Results for plain UHPC mixtures with and without 20% LP are shown in Figure 20a, and for fiber-reinforced UHPC mixtures in Figure 20b.

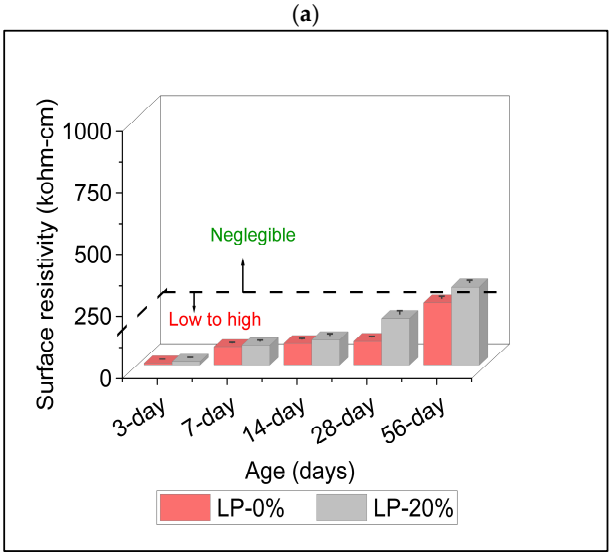
From Figure 20a, the SR values at fifty-six days for plain UHPC mixtures varied noticeably with the addition of LP. The plain UHPC mixture without LP exhibited an SR value of 558 kΩ·cm, while the mixture with 20% LP reached 707 kΩ·cm. Similarly, Figure 20b shows SR values of 252 kΩ·cm for fiber-reinforced UHPC without LP and 444 kΩ·cm with 20% LP. These results indicate that the presence of steel fibers reduces electrical resistivity, lowering SR values. However, even with fibers, the fifty-six-day SR values under MC remained above 234 kΩ·cm, suggesting that LP had only a minimal adverse effect on electrical resistivity.

For plain UHPC mixtures, replacing 20% cement with LP increased the SR value by 26.70% compared to the mixture without LP. This improvement aligns with earlier observations in this study, which noted the beneficial role of LP in refining pore structure and enhancing resistivity.

A consistent increase in SR values with curing age was also observed. To quantify this relationship, a linear regression analysis between SR values and curing duration for plain UHPC mixtures is presented in Figure 21. The results yielded strong correlations, with $R^2 = 0.98$ for mixtures without LP and $R^2 = 0.99$ for mixtures with 20% LP, indicating that SR increases linearly with curing time.



(**a**)



(**b**)

Figure 20. Surface resistivity values of UHPC mixtures without LP and with 20% LP for (**a**) plain UHPC mixtures and (**b**) fiber-reinforced UHPC mixtures, cured under MC regimen for 56 days.

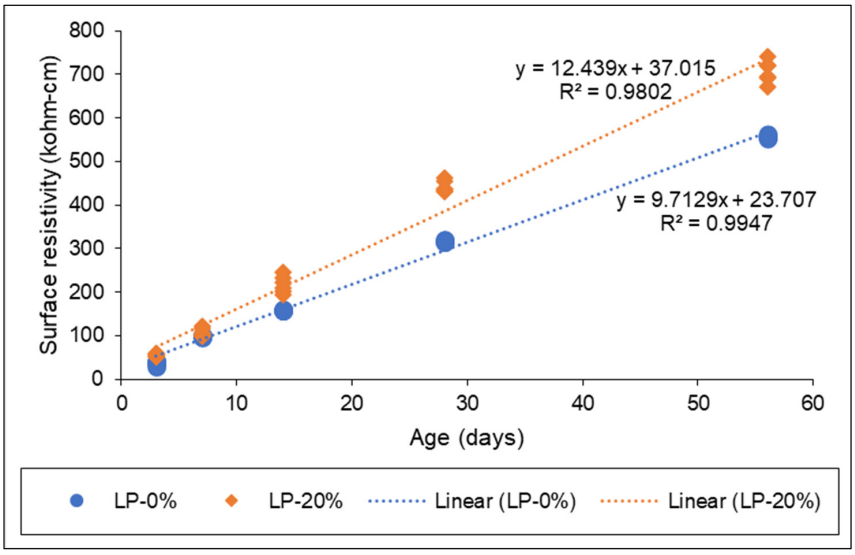


Figure 21. Linear relationship between curing age and surface resistivity values for UHPC mixtures without GGBFS containing 0% and 20% LP dosage.

3.10. Rapid Chloride Permeability Test

The charge passed values for plain UHPC mixtures with and without LP, cured for 56 days under MC and WB curing regimens, are presented in Figure 22. The control plain UHPC mixture without LP demonstrated very low chloride ion penetrability, with charge passed values ranging from 100 to 1000 Coulombs across curing conditions. For plain UHPC mixtures with 20% LP cured under MC regimen, the RCPT value was 139 Coulombs—14.38% lower than the plain UHPC mixture without LP under the same curing condition. Similarly, for plain UHPC mixtures with 20% LP cured under WB regimen, the RCPT value was 408 Coulombs—23.45% lower than the plain UHPC mixture without LP under WB curing. These results highlight the beneficial effect of LP as a cement substitute in enhancing the chloride resistance of UHPC mixtures.

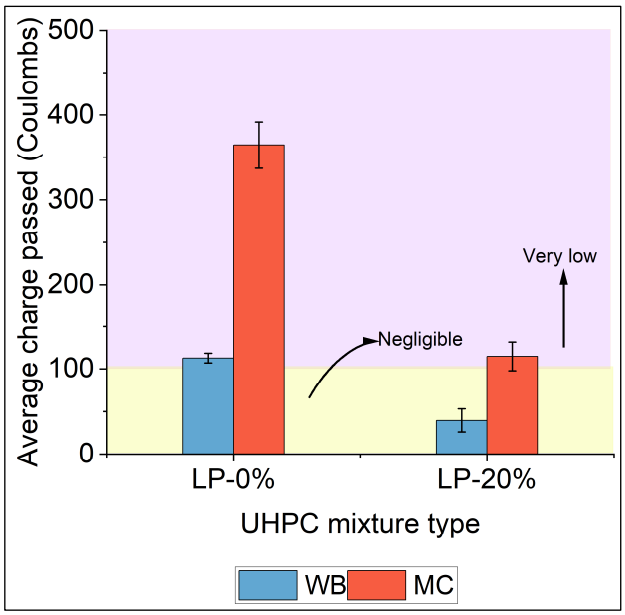


Figure 22. Average RCPT values for plain UHPC mixtures without LP and with 20% LP under MC and WB curing regimens at 56 days.

3.11. Microstructural Basis of Mechanical and Durability Behavior

Previous investigations using scanning electron microscopy (SEM), X-ray diffraction (XRD), and mercury intrusion porosimetry (MIP) have shown that UHPC possesses an exceptionally dense binder matrix and interfacial transition zone (ITZ) when fillers and supplementary materials are incorporated. Bahmani and Mostofinejad [75] reported that SEM images of UHPC matrices show an almost complete absence of large capillary pores and the presence of a continuous C–S–H gel network, which together account for UHPC's high strength and low permeability.

Studies on limestone-containing UHPC confirm that $CaCO_3$-rich fillers provide both physical and chemical benefits. Chen et al. [76] observed that LP acts as a nucleation site for C–S–H formation and participates in secondary reactions with aluminate phases, producing monocarboaluminate and hemicarboaluminate that densify the matrix. Dong et al. [77] reported similar outcomes in UHPC containing limestone and calcined clay, where SEM and XRD analyses confirmed a tighter microstructure and lower intensity of CH peaks, consistent with enhanced hydration and reduced porosity.

Additional microstructural investigations have linked durability improvements directly to pore structure refinement. Hernández-Carrillo et al. [78] further confirmed that limestone fillers promote a denser paste and ITZ morphology, improving the ho-

mogeneity of the matrix but slightly decreasing compressive strength due to the dilution of reactive phases.

These microstructural findings align with the present results. The moderate decline in strength observed with 20% LP replacement can be attributed to the dilution of reactive phases that limits total C–S–H production. In contrast, the filler-nucleation and carboaluminate-forming effects of LP refine pore structure, reduce ionic transport paths, and enhance surface resistivity and freeze–thaw durability. Collectively, the evidence supports that the mechanical and durability behavior of LP-modified UHPC is governed by a balance between chemical dilution and physical densification mechanisms, as also described in earlier limestone-based cement systems [76,78,79].

4. Sustainability

Cost and CO_2 Emissions Analysis

To assess the sustainability of the developed sustainable UHPC, both environmental and economic impacts were analyzed. This included a comparative evaluation of the embodied CO_2 emissions and the associated costs for UHPC mixtures with varying dosages of LP of 0% and 20%. This part of the study provides an indicative comparison of the environmental and economic implications of LP incorporation in UHPC. The cost values (Table 4) and CO_2 emissions (Table 5) were derived from published datasets and literature sources that report cost and emission factors for individual materials (cement, LP, silica fume, fly ash, superplasticizer, and steel fibers) respectively. The boundaries of the analysis were limited to material production and did not include transportation, processing energy, or curing energy inputs, which can vary significantly depending on regional supply chains and manufacturing practices. The results therefore represent a relative comparison between mixtures with and without LP. The total embodied CO_2 emissions for each UHPC mixture were calculated by multiplying the CO_2 emission factor of each constituent material by its quantity in the mixture, then summing the results.

Table 4. Cost of UHPC components taken from [60,80–82].

Materials Used	Cost $US/ton	References
Cement	82–110	[80,81]
Silica fume	350–1100	[80,81]
Fly ash	46–60	[80]
LP	122–124	[80]
HRWRA	3400	[81]
Steel fibers	5000	[81]
Natural river sand	100	[60]

Table 5. Emission factors of the materials used for the development of UHPC mixtures presented in this study.

Materials	CO_2 Emission (kg of CO_2/ton)	References
Cement	930	[17]
Fly ash	28	[83]
Silica fume	4–27	[84]
Fine aggregates	13.9	[83]
Limestone powder	17	[17]

Table 5. *Cont.*

Materials	CO_2 Emission (kg of CO_2/ton)	References
Superplasticizer	944	[85]
Fibers	1600	[85]

The cost results for plain and fiber-reinforced UHPC mixtures are shown in Figure 23. The material cost of UHPC mixtures with 20% LP was \$242/m^3 (\$317/yd^3) for plain UHPC and \$622/m^3 (\$814/yd^3) for fiber-reinforced UHPC. The replacement of 20% cement with LP reduced material costs by 4.5% and 2.0% for plain and fiber-reinforced mixtures, respectively. The inclusion of steel fibers significantly increased costs compared to plain mixtures, but the relative cost reduction from LP replacement remained evident.

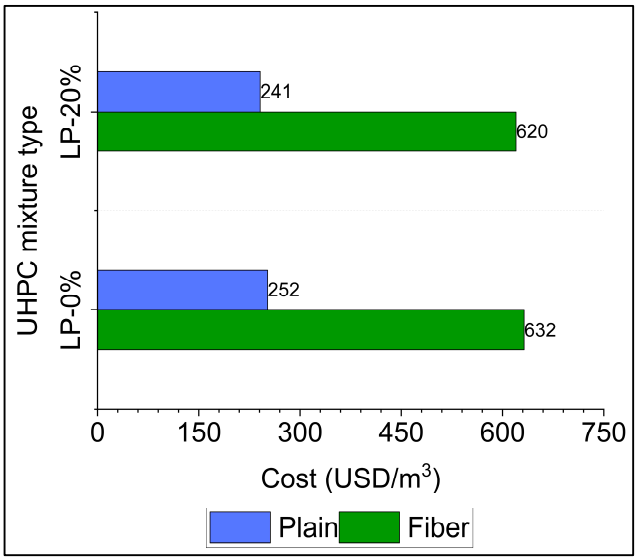


Figure 23. Cost of UHPC mixture with and without 20% LP for both plain and fiber-reinforced mixtures.

These findings indicate that LP is economically beneficial for both plain and fiber-reinforced UHPC while maintaining performance. The CO_2 emissions results are shown in Figure 24, while the combined cost–CO_2 analysis is presented in Figure 25.

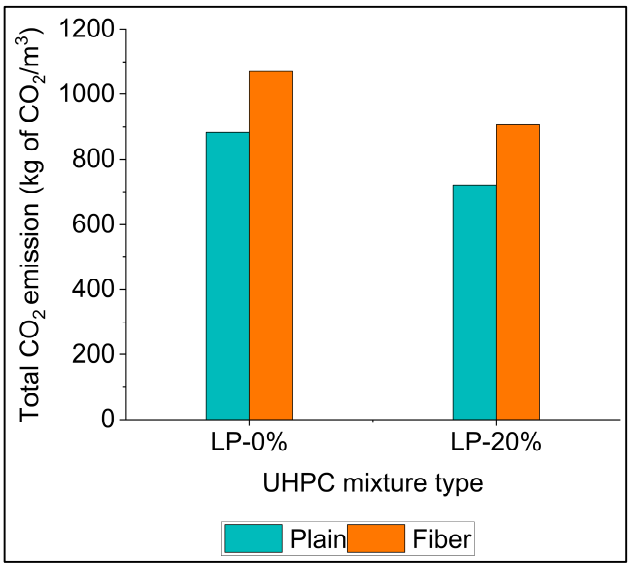


Figure 24. CO_2 emission of UHPC mixture with and without 20% LP.

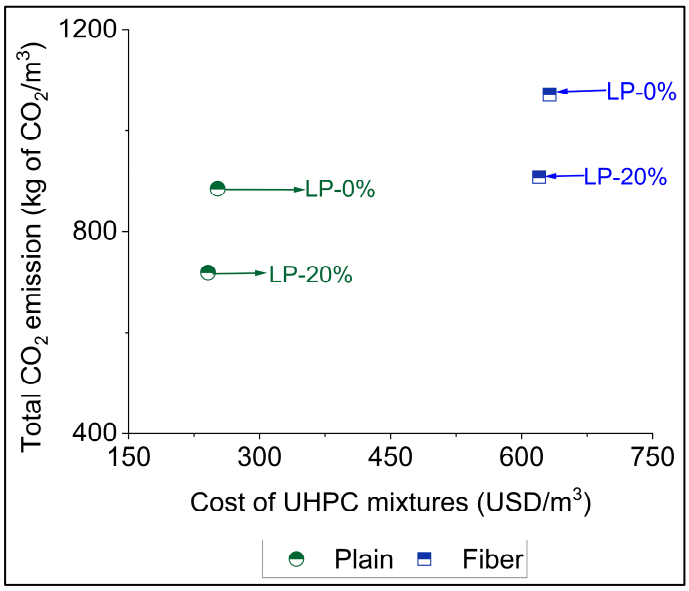


Figure 25. Relationship between material cost and total CO_2 emissions for all UHPC mixtures evaluated in this study.

For plain UHPC mixtures, the use of 20% LP reduced CO_2 emissions by 18.80% compared to mixtures without LP. Similarly, for fiber-reinforced UHPC, replacing 20% of cement with LP resulted in a 15.50% reduction in CO_2 emissions. Fiber-reinforced UHPC mixtures inherently had higher CO_2 emissions than plain UHPC due to the emissions associated with steel fiber production. Nonetheless, LP replacement mitigated part of this increase.

While this simplified approach allows for rapid benchmarking of the potential CO_2 savings associated with LP substitution, it does not capture the full environmental footprint of UHPC production. A more comprehensive evaluation—covering transportation, energy consumption during curing, and end-of-life stages—would provide deeper insight into the true sustainability performance of UHPC systems. Such an expanded boundary analysis could form the basis of future research focusing on the life-cycle implications of curing regimes and cement replacement strategies in UHPC.

5. Discussion

The results indicate that incorporating 20% LP as a cement replacement in UHPC influences both mechanical and durability performance through a combination of physical and chemical mechanisms. The modest reductions in compressive, tensile, and flexural strengths observed can be attributed primarily to the dilution effect, wherein partial replacement of reactive clinker phases (C_3S and C_2S) with relatively inert $CaCO_3$ particles reduces the quantity of hydration products such as calcium silicate hydrate (C–S–H) [26,50]. As a result, the total binding phase volume and overall matrix strength decrease. This early-age behavior is consistent with findings for composite Portland cements containing limestone filler and calcined clays, where dilution dominates the initial hydration phase [22,26].

Despite this dilution, the fine LP particles act as microfillers and nucleation sites, promoting the early precipitation of C–S–H and enhancing packing density within the UHPC matrix [17,23]. The higher specific surface area and improved particle packing reduce the volume of larger capillary pores, leading to a denser microstructure. At later ages, limited chemical interactions between LP and the aluminate phases of cement promote the formation of carboaluminate phases, particularly monocarboaluminate and hemicarboaluminate [68,86]. These secondary products fill voids and refine the pore net-

work, partially compensating for the reduction in C–S–H formation. Similar observations of carboaluminate stabilization and microstructural densification with $CaCO_3$ addition have been reported in high-performance and blended cements by Huang et al. [86] and Irassar E. F. [68].

The improved durability performance—including a lower charge passed in the RCPT test, higher surface resistivity, and excellent freeze–thaw resistance—can be explained by this refined pore structure. LP particles act as nucleation centers for C–S–H growth, which reduces pore interconnectivity and limits ionic transport pathways [87,88]. The increased electrical resistivity and reduced chloride penetrability suggest that LP incorporation decreases both total porosity and the connectivity of capillary pores, consistent with earlier microstructural analyses of limestone-containing UHPC [17,20]. Furthermore, finer pore sizes lower the amount of freezable water in the matrix, mitigating hydraulic pressure buildup during freezing cycles and thereby enhancing freeze–thaw durability [50,74].

In addition, LP improves matrix homogeneity and densifies the ITZ between paste and fibers. A denser ITZ reduces stress concentrations during mechanical loading and minimizes microcrack initiation, which may help preserve ductility and toughness despite slight reductions in ultimate strength [54,55].

Overall, using 20% LP in UHPC creates a balance between chemical and physical effects. Replacing part of the cement reduces the amount of hydration products, which slightly lowers strength, but the LP particles help fill voids, improve particle packing, and make the internal structure denser. This denser structure improves durability by reducing the pathways for water and ions to move through the concrete. As a result, LP-modifi0ed UHPC maintains strength while showing better resistance to chloride penetration and freeze–thaw damage. These outcomes align with previous studies on limestone-based high-performance concretes [17,42,43,67] and show that improving the microstructure—rather than depending only on binder reactivity—is key to achieving high performance and sustainability in UHPC.

6. Conclusions

This study evaluated the influence of partial cement replacement with LP on the fresh, mechanical, durability, and microstructural properties of UHPC. The results indicate that LP acts predominantly as an inert filler and hydration nucleation site, improving particle packing and enhancing mix workability without significantly affecting compressive strength. At a replacement level of 20%, LP improved flow by reducing internal friction and promoting better fiber dispersion, leading to a denser, more homogeneous matrix.

A moderate reduction in compressive, tensile and flexural strengths was observed at higher LP content, primarily due to dilution of reactive clinker phases. However, the mechanical performance remained within the range typical for UHPC applications, as microstructural refinement and filler effects partly compensated for reduced binder reactivity. The addition of LP also reduced both autogenous and drying shrinkage. The observed reduction in autogenous and drying shrinkage for UHPC mixtures with 20% LP may be linked to the lower heat evolution during hydration [23] and the refinement of the pore structure caused by the filler effect of LP. These mechanisms have been described in previous studies on limestone-modified cement systems by De Weerdt et al. [89] and general review on SCM by Juenger and Siddique [90]. Enhanced resistance to chloride ion penetration and freeze–thaw cycles further support the development of a dense and stable ITZ.

From a sustainability perspective, LP incorporation significantly reduces cement consumption and associated CO_2 emissions while maintaining the desired balance between strength, durability, and dimensional stability. Overall, replacing up to 20% of cement

with LP provides an optimal synergy between performance and environmental efficiency, confirming LP as a viable material for producing cost-effective and sustainable UHPC. Future research should explore long-term shrinkage evolution and durability mechanisms to further advance LP-modified UHPC for infrastructure applications.

Author Contributions: Conceptualization, S.A.; Methodology, S.A.; Validation, Y.S.; Formal analysis, Y.S. and S.A.; Investigation, Y.S.; Resources, S.A.; Data curation, Y.S. and M.Y.; Writing—original draft, Y.S.; Writing—review & editing, M.Y. and S.A.; Visualization, Y.S. and M.Y.; Supervision, S.A.; Project administration, S.A. All authors have read and agreed to the published version of the manuscript.

Funding: The research received no external funding.

Data Availability Statement: The original contributions presented in this study are included in the article. Further inquiries can be directed to the corresponding author.

Acknowledgments: The authors gratefully acknowledge Master Builders Solutions for their generous donation of admixtures and for conducting the particle size distribution analysis.

Conflicts of Interest: The authors declare that they have no known competing financial interests or personal relationships that could have appeared to influence the work reported in this paper.

References

1. Richard, P.; Cheyrezy, M.H. Reactive Powder Concretes With High Ductility and 200-800 MPa Compressive Strength. In *Proceedings of the V. Mohan Malhotra Symposium*; Mehta, P.K., Ed.; ACI SP 144-24; Victoria Wieczorek: Detroit, MI, USA, 1994; pp. 507–518.
2. Dili, A.S.; Santhanam, M. Investigations on Reactive Powder Concrete: A Developing Ultra High Strength Technology. *Indian Concr. J.* **2004**, *78*, 33–38.
3. Collepardi, S.; Coppola, L.; Troli, R.; Collepardi, M. Mechanical properties of modified reactive powder concrete. *ACI Spec. Publ.* **1997**, *173*, 1–22.
4. Richard, P.; Cheyrezy, M. Composition of reactive powder concretes. *Cem. Concr. Res.* **1995**, *25*, 1501–1511. [CrossRef]
5. Rossi, P. Influence of fibre geometry and matrix maturity on the mechanical performance of ultra high-performance cement-based composites. *Cem. Concr. Compos.* **2013**, *37*, 246–248.
6. Hasan, T.; Gilbert, L.; Allena, S.; Owusu-Danquah, J.; Torres, A. Development of non-proprietary ultra-high performance concrete mixtures. *Buildings* **2022**, *12*, 1865.
7. Worrell, E.; Price, L.; Martin, N.; Hendriks, C.; Meida, L.O. Carbon dioxide emissions from the global cement industry. *Annu. Rev. Energy Environ.* **2001**, *26*, 303–329. [CrossRef]
8. Yu, R.; Spiesz, P.; Brouwers, H.J.H. Mix design and properties assessment of ultra-high performance fibre reinforced concrete (UHPFRC). *Cem. Concr. Res.* **2014**, *56*, 29–39. [CrossRef]
9. Korpa, A.; Kowald, T.; Trettin, R. Phase development in normal and ultra high performance cementitious systems by quantitative X-ray analysis and thermoanalytical methods. *Cem. Concr. Res.* **2009**, *39*, 69–76. [CrossRef]
10. Li, S.; Cheng, S.; Mo, L.; Deng, M. Effects of steel slag powder and expansive agent on the properties of ultra-high performance concrete (UHPC): Based on a case study. *Materials* **2020**, *13*, 683. [CrossRef]
11. Ahmad, S.; Hakeem, I.; Maslehuddin, M. Development of UHPC Mixtures Utilizing Natural and Industrial Waste Materials as Partial Replacements of Silica Fume and Sand. *Sci. World J.* **2014**, *2014*, 713531. [CrossRef]
12. Wetzel, A.; Middendorf, B. Influence of silica fume on properties of fresh and hardened ultra-high performance concrete based on alkali-activated slag. *Cem. Concr. Compos.* **2019**, *100*, 53–59.
13. Jing, R.; Liu, Y.; Yan, P. Uncovering the effect of fly ash cenospheres on the macroscopic properties and microstructure of ultra high-performance concrete (UHPC). *Constr. Build. Mater.* **2021**, *286*, 122977. [CrossRef]
14. Duval, R.; Kadri, E.H. Influence of silica fume on the workability and the compressive strength of high-performance concretes. *Cem. Concr. Res.* **1998**, *28*, 533–547. [CrossRef]
15. Jiang, Z.; Sun, Z.; Wang, P.; Wang, X. Study on self-desiccation effect of high performance concrete. *J. Build. Mater.* **2004**, *7*, 19–24.
16. Jensen, M.; Hansen, P.F. Autog enous deformation and change of the relative humidity in silica fume-modified cement paste. *Mater. J.* **1996**, *93*, 539–543.
17. Li, P.P.; Brouwers, H.J.H.; Chen, W.; Yu, Q. Optimization and characterization of high-volume limestone powder in sustainable ultra-high performance concrete. *Constr. Build. Mater.* **2020**, *242*, 118112. [CrossRef]

18. Park, S.; Wu, S.; Liu, Z.; Pyo, S. The role of supplementary cementitious materials (SCMs) in ultra high performance concrete (UHPC): A review. *Materials* **2021**, *14*, 1472. [CrossRef]
19. Yeluri, M.; Ertugral, E.; Sharma, Y.; Fodor, P.; Kothapalli, C.; Allena, S. Revolutionizing ultra-high performance concrete: Unleashing metakaolin and diatomaceous earth as sustainable fly ash alternatives. *Constr. Build. Mater.* **2025**, *460*, 139822. [CrossRef]
20. Wang, D.; Shi, C.; Farzadnia, N.; Shi, Z.; Jia, H.; Ou, Z. A review on use of limestone powder in cement-based materials: Mechanism, hydration and microstructures. *Constr. Build. Mater.* **2018**, *181*, 659–672. [CrossRef]
21. Huang, W.; Kazemi-Kamyab, H.; Sun, W.; Scrivener, K. Effect of replacement of silica fume with calcined clay on the hydration and microstructural development of eco-UHPFRC. *Mater. Des.* **2017**, *121*, 36–46. [CrossRef]
22. Wang, D.; Shi, C.; Farzadnia, N.; Shi, Z.; Jia, H. A review on effects of limestone powder on the properties of concrete. *Constr. Build. Mater.* **2018**, *192*, 153–166. [CrossRef]
23. Bentz, D.P.; Ferraris, C.F.; Jones, S.Z.; Lootens, D.; Zunino, F. Limestone and silica powder replacements for cement: Early-age performance. *Cem. Concr. Compos.* **2017**, *78*, 43–56. [CrossRef]
24. Zhuang, W.; Li, S.; Wang, Z.; Zhang, Z.; Yu, Q. Impact of micromechanics on dynamic compressive behavior of ultra-high performance concrete containing limestone powder. *Compos. Part B Eng.* **2022**, *243*, 110160. [CrossRef]
25. Li, P.P.; Cao, Y.Y.Y.; Brouwers, H.J.H.; Chen, W.; Yu, Q.L. Development and properties evaluation of sustainable ultra-high performance pastes with quaternary blends. *J. Clean. Prod.* **2019**, *240*, 118124. [CrossRef]
26. Bonavetti, V.; Donza, H.; Menéndez, G.; Cabrera, O.; Irassar, E.F. Limestone filler cement in low w/c concrete: A rational use of energy. *Cem. Concr. Res.* **2003**, *33*, 865–871. [CrossRef]
27. Yang, R.; Yu, R.; Shui, Z.; Gao, X.; Han, J.; Lin, G.; Qian, D.; Liu, Z.; He, Y. Environmental and economical friendly ultra-high performance-concrete incorporating appropriate quarry-stone powders. *J. Clean. Prod.* **2020**, *260*, 121112. [CrossRef]
28. Ding, M.; Yu, R.; Geng, Y.; Wang, S.; Zhou, F.; Shui, Z.; Gao, X.; He, Y.; Chen, L. Possibility and advantages of producing an ultra-high performance concrete (UHPC) with ultra-low cement content. *Constr. Build. Mater.* **2021**, *273*, 122023. [CrossRef]
29. Thomas, M. *Supplementary Cementing Materials in Concrete*; CRC Press: Boca Raton, FL, USA, 2013.
30. Siddique, R. Utilization of silica fume in concrete: Review of hardened properties. *Resour. Conserv. Recycl.* **2011**, *55*, 923–932. [CrossRef]
31. Ullah, R.; Qiang, Y.; Ahmad, J.; Vatin, N.I.; El-Shorbagy, M.A. Ultra-high-performance concrete (UHPC): A state-of-the-art review. *Materials* **2022**, *15*, 4131. [CrossRef]
32. Sharma, Y.; Yeluri, M.; Allena, S.; Owusu-Danquah, J. Incorporating Limestone Powder and Ground Granulated Blast Furnace Slag in Ultra-high Performance Concrete to Enhance Sustainability. *Int. J. Concr. Struct. Mater.* **2024**, *18*, 79. [CrossRef]
33. *ASTM C1437-20*; Standard Test Method for Flow of Hydraulic Cement Mortar. ASTM International: West Conshohocken, PA, USA, 2020. [CrossRef]
34. *ASTM C109*; Standard Test Method for Compressive Strength of Hydraulic Cement Mortars (Using 2-in. or [50-mm] Cube Specimens). ASTM International: West Conshohocken, PA, USA, 2020.
35. *ASTM C496/C496M-17*; Standard Test Method for Splitting Tensile Strength of Cylindrical Concrete Specimens. ASTM International: West Conshohocken, PA, USA, 2017.
36. *ASTM C469-02*; Standard Test Method for Static Modulus of Elasticity and Poisson's Ratio of Concrete in Compression. ASTM International: West Conshohocken, PA, USA, 2017.
37. *ASTM C1609/C1609M-19a*; Standard Test Method for Flexural Performance of Fiber-Reinforced Concrete (Using Beam With Third-Point Loading). ASTM International: West Conshohocken, PA, USA, 2019.
38. Graybeal, B.; Baby, F.; Marchand, P.; Toutlemonde, F. Direct and flexural tension test methods for determination of the tensile stress-strain response of UHPFRC. In Proceedings of the Kassel International Conference, Hipermat, Kassel, Germany, 7–9 March 2012; pp. 395–418.
39. ASTM C157/C157M-17; Standard Test Method for Length Change of Hardened Hydraulic-Cement Mortar and Concrete. ASTM International: West Conshohocken, PA, USA, 2017. [CrossRef]
40. *ASTM C1202-19*; Standard Test Method for Electrical Indication of Concrete's Ability to Resist Chloride Ion Penetration. ASTM International: West Conshohocken, PA. USA, 2019.
41. *AASHTO TP95-11*; Standard Method of Test for Surface Resistivity Indication of Concrete's Ability to Resist Chloride Ion Penetration. American Association of State Highway and Transportation Officials: Washington, DC, USA, 2011.
42. *ASTM C666/C666M-15*; Standard Test Method for Resistance of Concrete to Rapid Freezing and Thawing. ASTM International: West Conshohocken, PA, USA, 2015.
43. Kang, S.T.; Kim, J.K. Investigation on the flexural behavior of UHPCC considering the effect of fiber orientation distribution. *Constr. Build. Mater.* **2012**, *28*, 57–65. [CrossRef]
44. Kang, S.T.; Lee, B.Y.; Kim, J.K.; Kim, Y.Y. The effect of fibre distribution characteristics on the flexural strength of steel fibre-reinforced ultra high strength concrete. *Constr. Build. Mater.* **2011**, *25*, 2450–2457. [CrossRef]

45. Wu, Z.; Khayat, K.H.; Shi, C. Changes in rheology and mechanical properties of ultra-high performance concrete with silica fume content. *Cem. Concr. Res.* **2019**, *123*, 105786. [CrossRef]
46. Wille, K.; El-Tawil, S.; Naaman, A.E. Properties of strain hardening ultra high performance fiber reinforced concrete (UHP-FRC) under direct tensile loading. *Cem. Concr. Compos.* **2014**, *48*, 53–66. [CrossRef]
47. Meng, W.; Khayat, K.H. Mechanical properties of ultra-high-performance concrete enhanced with graphite nanoplatelets and carbon nanofibers. *Compos. Part B: Eng.* **2016**, *107*, 113–122.
48. Sersale, R. Advances in Portland and blended cements. In Proceedings of the 9 th International Congress on the Chemistry of Cement, New Delhi, India, 23–28 November 1992.
49. Cyr, M.; Lawrence, P.; Ringot, E. Efficiency of mineral admixtures in mortars: Quantification of the physical and chemical effects of fine admixtures in relation with compressive strength. *Cem. Concr. Res.* **2006**, *36*, 264–277. [CrossRef]
50. Gong, C.; Zhou, X.; Ji, L.; Dai, W.; Lu, L.; Cheng, X. Effects of limestone powders on pore structure and physiological characteristics of planting concrete with sulfoaluminate cement. *Constr. Build. Mater.* **2018**, *162*, 314–320. [CrossRef]
51. Jin, W.; Tang, X.; Bai, Z.; Yang, H.; Chen, Z.; Wang, L.; Zhang, L.; Jiang, L. Effect of Curing Temperature on Mechanical Strength and Thermal Properties of Hydraulic Limestone Powder Concrete. *J. Mater. Eng. Perform.* **2023**, *33*, 11214–11230. [CrossRef]
52. *ASTM C1856*; Standard Practice for Fabricating and Testing Specimens of Ultra-High Performance Concrete. ASTM International: West Conshohocken, PA, USA, 2024.
53. Shi, X.S.; Collins, F.G.; Zhao, X.L.; Wang, Q.Y. Mechanical properties and microstructure analysis of fly ash geopolymeric recycled concrete. *J. Hazard. Mater.* **2012**, *237*, 20–29. [CrossRef] [PubMed]
54. Çakır, Ö. Experimental analysis of properties of recycled coarse aggregate (RCA) concrete with mineral additives. *Constr. Build. Mater.* **2014**, *68*, 17–25. [CrossRef]
55. Wong, H.S.; Zobel, M.; Buenfeld, N.R.; Zimmerman, R.W. Influence of the interfacial transition zone and microcracking on the diffusivity, permeability and sorptivity of cement-based materials after drying. *Mag. Concr. Res.* **2009**, *61*, 571–589. [CrossRef]
56. Demirhan, S.; Turk, K.; Ulugerger, K. Fresh and hardened properties of self consolidating Portland limestone cement mortars: Effect of high volume limestone powder replaced by cement. *Constr. Build. Mater.* **2019**, *196*, 115–125. [CrossRef]
57. Zhang, P.; Wang, C.; Gao, Z.; Wang, F. A review on fracture properties of steel fiber reinforced concrete. *J. Build. Eng.* **2023**, *67*, 105975. [CrossRef]
58. Hu, Y.; Chen, J.; Zou, F.; He, M.; Mao, J.; Liu, X.; Zhou, C.; Yuan, Z. A comparative study of temperature of mass concrete placed in August and November based on on-site measurement. *Case Stud. Constr. Mater.* **2021**, *15*, e00694. [CrossRef]
59. Toutanji, H.A.; Bayasi, Z. Effect of curing procedures on properties of silica fume concrete. *Cem. Concr. Res.* **1999**, *29*, 497–501. [CrossRef]
60. Shah, H.A.; Yuan, Q.; Photwichai, N. Use of materials to lower the cost of ultra-high-performance concrete–A review. *Constr. Build. Mater.* **2022**, *327*, 127045. [CrossRef]
61. Smarzewski, P. Study of toughness and macro/micro-crack development of fibre-reinforced ultra-high performance concrete after exposure to elevated temperature. *Materials* **2019**, *12*, 1210. [CrossRef]
62. Russell, H.G.; Graybeal, B.A. *Ultra-High Performance Concrete: A state-of-the-Art Report for the Bridge Community (No. FHWA-HRT-13-060)*; United States. Department of Transportation. Federal Highway Administration; Office of Infrastructure Research and Development: Washington, DC, USA, 2013.
63. Nayar, S.K.; Gettu, R.; Krishnan, S. Characterisation of the toughness of fibre reinforced concrete–revisited in the Indian context. *Indian Concr. J.* **2014**, *88*, 8–23.
64. Rashiddadash, P.; Ramezanianpour, A.A.; Mahdikhani, M. Experimental investigation on flexural toughness of hybrid fiber reinforced concrete (HFRC) containing metakaolin and pumice. *Constr. Build. Mater.* **2014**, *51*, 313–320. [CrossRef]
65. Liu, F.; Ding, W.; Qiao, Y. Experimental investigation on the flexural behavior of hybrid steel-PVA fiber reinforced concrete containing fly ash and slag powder. *Constr. Build. Mater.* **2019**, *288*, 116706. [CrossRef]
66. Mehta, P.K.; Monteiro, P. *Concrete: Structure, Properties and Materials*, 2nd ed.; McGraw-Hill: NewYork, NY, USA, 1995.
67. Shen, P.; Lu, L.; He, Y.; Wang, F.; Hu, S. The effect of curing regimes on the mechanical properties, nano-mechanical properties and microstructure of ultra-high performance concrete. *Cem. Concr. Res.* **2019**, *118*, 1–13. [CrossRef]
68. Irassar, E.F. Sulfate attack on cementitious materials containing limestone filler—A review. *Cem. Concr. Res.* **2009**, *39*, 241–254. [CrossRef]
69. Mohebbi, A.; Graybeal, B.; Haber, Z. Time-dependent properties of ultrahigh-performance concrete: Compressive creep and shrinkage. *J. Mater. Civ. Eng.* **2022**, *34*, 04022096. [CrossRef]
70. Tuan, N.V.; Ye, G.; van Breugel, K. Mitigation of early age shrinkage of ultra high performance concrete by using rice husk ash. In Proceedings of the 3rd International Symposium on UHPC and Nanotechnology for High Performance Construction Materials: Ultra-High Performance Concrete and Nanotechnology in Construction (HIPERMAT-2012), Kassel, Germany, 7–9 March 2012.
71. Wu, Z.; Shi, C.; Khayat, K.H.; Wu, Z.; Shi, C.; Khayat, K.H. Investigation of mechanical properties and shrinkage of ultra-high performance concrete: Influence of steel fiber content and shape. *Compos. Part B Eng.* **2019**, *174*, 107021. [CrossRef]

72. Fu, D.; Xia, C.; Xu, S.; Zhang, C.; Jia, X. Effect of concrete composition on drying shrinkage behavior of ultra-high performance concrete. *J. Build. Eng.* **2022**, *62*, 105333. [CrossRef]
73. Ahmad, I.; Shen, D.; Khan, K.A.; Jan, A.; Khubaib, M.; Ahmad, T.; Nasir, H. Effectiveness of limestone powder in controlling the shrinkage behavior of cement based system: A review. *Silicon* **2009**, *31*, 715–720. [CrossRef]
74. Muro-Villanueva, J.; Newtson, C.M.; Weldon, B.D.; Jauregui, D.V.; Allena, S. Freezing and thawing durability of ultra high strength concrete. *J. Civ. Eng. Arch.* **2013**, *7*, 907. [CrossRef]
75. Bahmani, H.; Mostofinejad, D. Microstructure of ultra-high-performance concrete (UHPC)–a review study. *J. Build. Eng.* **2022**, *50*, 104–118. [CrossRef]
76. Chen, M.; He, Y.; Lü, L.; Zhang, X. Effect of High Content Limestone Powder on Microstructure and Mechanical Properties of Cement-based Materials. *J. Wuhan Univ. Technol. Sci. Ed.* **2023**, *38*, 557–566. [CrossRef]
77. Dong, Y.; Liu, Y.; Hu, C. owards greener ultra-high performance concrete based on highly-efficient utilization of calcined clay and limestone powder. *Build. Eng.* **2023**, *66*, 105836. [CrossRef]
78. Hernández-Carrillo, G.; Durán-Herrera, A.; Tagnit-Hamou, A. Effect of limestone and quartz fillers in UHPC with calcined clay. *Materials* **2022**, *15*, 7711. [CrossRef]
79. Luan, C.; Yang, Q.; Lin, X.; Gao, X.; Cheng, H.; Huang, Y.; Du, P.; Zhou, Z.; Wang, J. The synergistic effects of ultrafine slag powder and limestone on the rheology behavior, microstructure, and fractal features of ultra-high performance concrete (UHPC). *Materials* **2023**, *16*, 2281. [CrossRef]
80. Wille, K.; Boisvert-Cotulio, C. Material efficiency in the design of ultra-high performance concrete. *Constr. Build. Mater.* **2015**, *86*, 33–43. [CrossRef]
81. Alsalman, A.; Dang, C.N.; Martí-Vargas, J.R.; Hale, W.M. Mixture-proportioning of economical UHPC mixtures. *J. Build. Eng.* **2020**, *27*, 100970. [CrossRef]
82. Goldman, S.; Majsztrik, P.; Rojas, I.S.; Gavvalapalli, M. *Pathways to Commercial Liftoff: Low-Carbon Cement*; U.S. Department of Energy: Washington, DC, USA, 2023.
83. Flower, D.J.; Sanjayan, J. Green house gas emissions due to concrete manufacture. *Int. J. Life Cycle Assess.* **2007**, *12*, 282–288. [CrossRef]
84. King, D. The effect of silica fume on the properties of concrete as defined in concrete society report 74, cementitious materials. In Proceedings of the 37th Conference on Our World in Concrete and Structures, Singapore, 27–28 August 2012.
85. Mehdipour, S.; Nikbin, I.M.; Dezhampanah, S.; Mohebbi, R.; Moghadam, H.; Charkhtab, S.; Moradi, A. Mechanical properties, durability and environmental evaluation of rubberized concrete incorporating steel fiber and metakaolin at elevated temperatures. *J. Clean. Prod.* **2020**, *254*, 120126. [CrossRef]
86. Huang, W.; Kazemi-Kamyab, H.; Sun, W.; Scrivener, K. Effect of cement substitution by limestone on the hydration and microstructural development of ultra-high performance concrete (UHPC). *Cem. Concr. Compos.* **2017**, *77*, 86–101. [CrossRef]
87. Gesoğlu, M.; Güneyisi, E.; Kocabağ, M.E.; Bayram, V.; Mermerdaş, K. Fresh and hardened characteristics of self compacting concretes made with combined use of marble powder, limestone filler, and fly ash. *Constr. Build. Mater.* **2012**, *37*, 160–170. [CrossRef]
88. Li, L.G.; Kwan, A.K. Adding limestone fines as cementitious paste replacement to improve tensile strength, stiffness and durability of concrete. *Cem. Concr. Compos.* **2015**, *60*, 17–24. [CrossRef]
89. De Weerdt, K.; Kjellsen, K.O.; Sellevold, E.; Justnes, H. Synergy between fly ash and limestone powder in ternary cements. *Cem. Concr. Compos.* **2011**, *33*, 30–38. [CrossRef]
90. Juenger, M.C.; Siddique, R. Recent advances in understanding the role of supplementary cementitious materials in concrete. *Cem. Concr. Res.* **2015**, *78*, 71–80. [CrossRef]

Disclaimer/Publisher's Note: The statements, opinions and data contained in all publications are solely those of the individual author(s) and contributor(s) and not of MDPI and/or the editor(s). MDPI and/or the editor(s) disclaim responsibility for any injury to people or property resulting from any ideas, methods, instructions or products referred to in the content.